## DISCLAIMER

**This report was prepared as an account of work sponsored by an agency of the United States Government. Neither the United States Government nor any agency thereof, nor any of their employees, makes any warranty, express or implied, or assumes any legal liability or responsibility for the accuracy, completeness, or usefulness of any information, apparatus, product, or process disclosed, or represents that its use would not infringe privately owned rights. Reference herein to any specific commercial product, process, or service by trade name, trademark, manufacturer, or otherwise does not necessarily constitute or imply its endorsement, recommendation, or favoring by the United States Government or any agency thereof. The views and opinions of authors expressed herein do not necessarily state or reflect those of the United States Government or any agency thereof. Reference herein to any social initiative (including but not limited to Diversity, Equity, and Inclusion (DEI); Community Benefits Plans (CBP); Justice 40; etc.) is made by the Author independent of any current requirement by the United States Government and does not constitute or imply endorsement, recommendation, or support by the United States Government or any agency thereof.**


# Study of the Protection Improvements for a Weak Grid Area With High Inverter-Based Resources (IBRs)

Jing Wang,[1] Abu Shouaib Hasan,[1] Yaswanth Nag Velaga,[1] Lang Chen,[2] Joseph Dubeau,[2] and Andrew Arana[2]

*1 National Laboratory of the Rockies*
*2 Florida Power and Light*

**The National Laboratory of the Rockies is a national laboratory of the U.S. Department of Energy, Office of Critical Minerals and Energy Innovation, operated under Contract No. DE-AC36-08GO28308.**

This report is available at no cost from the National Laboratory of the Rockies (NLR) at www.nlr.gov/publications.

**Technical Report**
NLR/TP-5D00-98333
February 2026

NATIONAL LABORATORY OF THE ROCKIES

# Study of the Protection Improvements for a Weak Grid Area With High Inverter-Based Resources (IBRs)

Jing Wang,[1] Abu Shouaib Hasan,[1] Yaswanth Nag Velaga,[1] Lang Chen,[2] Joseph Dubeau,[2] and Andrew Arana[2]

*1 Florida Power and Light*

*2 National Laboratory of the Rockies*

**Suggested Citation**

Wang, Jing, Abu Shouaib Hasan, Yaswanth Nag Velaga, Lang Chen, Joseph Dubeau, and Andrew Arana. 2026. *Study of the Protection Improvements for a Weak Grid Area With High Inverter-Based Resources (IBRs)*. Golden, CO: National Laboratory of the Rockies. NREL/TP-5D00-98333. https://www.nlr.gov/docs/fy26osti/98333.pdf.

**The National Laboratory of the Rockies is a national laboratory of the U.S. Department of Energy, Office of Critical Minerals and Energy Innovation, operated under Contract No. DE-AC36-08GO28308.**

This report is available at no cost from the National Laboratory of the Rockies (NLR) at www.nlr.gov/publications.

**Technical Report**
NLR/TP-5D00-98333
February 2026

National Laboratory of the Rockies
15013 Denver West Parkway
Golden, CO 80401
303-275-3000 • www.nlr.gov

**NOTICE**

This work was authored in part by the National Laboratory of the Rockies for the U.S. Department of Energy (DOE), operated under Contract No. DE-AC36-08GO28308. Funding provided by Florida Power and Light. The views expressed herein do not necessarily represent the views of the DOE or the U.S. Government.

This report was produced when the laboratory operated as the National Renewable Energy Laboratory (NREL). The laboratory is now the National Laboratory of the Rockies (NLR).



*Cover photos (clockwise from left): Josh Bauer, National Laboratory of the Rockies 61725; Visualization from National Laboratory of the Rockies Insight Center; Getty-181828180; Agata Bogucka, National Laboratory of the Rockies 91683; Dennis Schroeder, National Laboratory of the Rockies 51331; Werner Slocum, National Laboratory of the Rockies 67842.*

# Acknowledgments

This work is based on work supported by Florida Power & Light Company and the U.S. Department of Energy Office of Critical Minerals and Energy Innovation Solar Energy Technologies Office.

The authors thank Guohui Yuan of the U.S. Department of Energy Office of Critical Minerals and Energy Innovation Solar Energy Technologies Office for his support and his very helpful insights for this study. We also thank Barry Mather from the National Laboratory of the Rockies for his support for this work.

In addition, we acknowledge the validated OEM model provided by Shahil Shah and his team from the National Laboratory of the Rockies, the support for this study provided by Soham Chakraborty from the National Laboratory of the Rockies, Brian Johnson from the University of Idaho, and the Siemens CAPE Technical Support Team. We also thank Siddharth Pant and Pooja Gupta from GE Vernova for providing the primary original equipment manufacturer models and Sai Gopal Vennelaganti and Fatemeh Sharifi from Tesla for providing the benchmark original equipment manufacturer black-box models for the study.

# List of Acronyms

| | |
|---|---|
| AG | phase-to-ground |
| BC | phase-to-phase |
| BCG | phase-to-phase-to-ground |
| CHIL | controller-hardware-in-the-loop |
| EMT | electromagnetic transient |
| GFL | grid following |
| GFM | grid forming |
| IBR | inverter-based resource |
| IEEE | Institute of Electrical and Electronics Engineers |
| L | line (e.g., L1, L2) |
| OEM | original equipment manufacturer |
| PV | photovoltaics |
| R | relay (e.g., R1, R2) |
| SCR | short-circuit ratio |
| SLG | single line to ground |

# Executive Summary

This report evaluates the protection schemes of Florida Power & Light Company's weak grid area with high penetrations of inverter-based resources (IBRs) and proposes strategies to enhance the protection system reliability of that weak grid area. This area is located in Florida Power & Light Company's 161-kV transmission system. The transmission line is 180 miles long, and it includes five solar plants that will be installed in three locations. Additionally, two large grid-forming (GFM) inverters will be installed in two solar locations. This weak grid area has a low short-circuit ratio (≤1.5), and the system potentially faces power system stability and protection system reliability issues because of the IBRs. This project evaluates the reliability of the protective relays and proposes modifications or enhancements to the protection system. The system we used for this study has only one solar plant (grid-following [GFL] inverters), and we evaluate how this solar plant will affect the existing protection schemes. Additionally, we evaluate the fault current response of the GFM battery energy storage system.

To evaluate the existing protection schemes, a relay hardware-in-the-loop experiment is performed in the laboratory using the relays and settings provided by the utility partner. Because the IBR black-box model cannot be embedded in the RTDS, we must use the replay approach: The RTDS recreates the COMTRADE fault data from PSCAD and connects with the hardware relays via inputs/outputs for the relay response testing. Note that PSCAD runs the power system model with the IBR black-box model because PSCAD can accurately capture/represent the IBR fault responses during transients for the relay response testing and performance evaluation. The PSCAD power system model is manually developed from the reduced CAPE model, and proper model validation is performed to ensure that the PSCAD model matches the CAPE model for the fault study and replay performance evaluation. The fault testing scenarios include normal, N-1 contingency, and IBR-only situations. Both the GFL and GFM IBR under testing have low and oscillatory fault currents, and they do not inject negative-sequence current. This nonstandard fault behavior significantly challenges traditional transmission line protection.

The key findings from this report include:

- The differential element of the SEL-411L relay operated reliably under all tested conditions, including normal operation, N-1 contingencies, and the inverter-based resource (IBR)–only scenario. The distance element (e.g., mho) and the directional element (e.g., 32Q) also performed reliably under normal conditions and N-1 contingencies; however, they failed to operate correctly in the IBR-only scenario due to the absence of regulated negative-sequence current injection from the IBRs.
- More specifically, when the IBR is the only source contributing fault current, the differential element operates reliably, but the distance and directional elements that rely on the regulated negative-sequence current and/or overcurrent misoperate. The affected protection relay elements are: (1) 32 Q, (2) Z1P/Z2P/Z1G/Z2G, and (3) some overcurrent supervision elements. The inability of these elements to correctly assert stems from the lack of negative-sequence current and a consistent I2-V2 phasor relationship ($I_2$ leads $V_2$ by approximately 90°).
- The proposed enhanced protection schemes aim to address the challenges of the lack of regulated negative sequence current from the IBRs. For ground faults, the increased restraining factors (a2 and k2) can quickly block the negative-sequence current-based

direction element and switch to the zero-sequence voltage-based direction element. Changing from the QV order to the V order has a similar effect but with a faster response because there is no waiting time for blacking the Q and switching to V. For phase-to-phase faults, the undervoltage and phase angle supervision elements are helpful to increase the selectivity and reliability of the mho distance element even with a low fault current. Those enhanced protection schemes are good references for other utility systems with similar problems.

- The second solution to solve the protection problems is to have the IBRs inject regulated negative-sequence current per the Institute of Electrical and Electronics Engineers (IEEE) Std. 2800-200; therefore, benchmark GFL and GFM inverters from another vendor are used, and both the GFL and GFM IBRs comply with the IEEE Std. 2800-2022 negative-sequence current requirement. Both models provide a high amount of negative-sequence current and have consistent negative-sequence current and negative-sequence voltage phasor relationships ($I_2$ leads $V_2$ by approximately 90°). These are beneficial for relays to continue to operate reliably; this is why the directional and distance elements operate reliably with a fast response for both the GFL-only and the GFL + GFM scenarios.
- In the real world, it is impractical for protection engineers to rerun fault studies and adjust the protection settings/logic to accommodate issues brought by IBRs. Requesting that the IBRs comply with IEEE Std. 2800-2022 is more doable. This should be included in interconnection studies and reviewed by protection engineers.

This project explores a framework to address the gaps in protection studies for high-IBR grids. The learnings and findings are good references for utilities that have similar challenges in power system protection. Today's grids have many traditional synchronous machines, but future grids with higher penetrations of IBRs will have increasingly more pronounced issues in power system protection. Further, the lack of negative-sequence current in IBRs is a common problem for protection systems. More attention and research efforts are needed to develop protection schemes that work reliably with and without negative sequence current injections.

# Table of Contents

# List of Figures

# List of Tables

# 1 Overview of the Protection System Study

## 1.1 Background

The integration of additional energy resources is fundamentally transforming the operation and protection of modern power systems. Florida Power & Light Company is undergoing a significant energy transition, with projections indicating the addition of approximately 25 GW of photovoltaic (PV) generation and 3.5 GW of nuclear capacity by 2032 to serve a peak summer load of 32 GW. Although this transition enhances energy diversity, it also introduces unprecedented technical challenges for system stability, reliability, and protection. A key concern stems from the rapid growth of inverter-based resources (IBRs), such as solar PV, which behave differently than conventional synchronous generators. The utility's site-dependent short-circuit ratio (SCR) map reveals that many regions of the grid operate with SCR values below 1.5, indicating weak grid conditions. Under such conditions, IBRs exhibit dynamic interactions with the network that can lead to degraded voltage stability, control oscillations, and reliability issues with traditional protection systems.

The utility has already encountered IBR performance issues, particularly related to fault ride-through capability and motor-starting problems. These operational experiences have raised important questions about the stability of electric grids and the continued reliability and sensitivity of existing protection schemes. Traditional relay settings and fault detection principles were developed for strong, synchronous-generator-dominated systems. They might not function as intended in grids characterized by low short-circuit levels and limited fault current contributions from IBRs. Within this context, it becomes essential to evaluate the effectiveness of the current protection schemes, especially in weak grid areas with high IBR penetrations. This assessment will help identify protection challenges, define enhancement needs for relay coordination and settings, and ensure that the protection system remains dependable and secure as the utility transitions toward an inverter-dominated electric grid.

## 1.2 Project Objectives

The primary objective of this study is to evaluate the performance and reliability of the existing protection schemes of the utility's weak grid area in their transmission system with high penetrations of IBRs and propose solutions to enhance the existing protection schemes. Specifically, the study aims to:

- Develop a power system network model with good representation of the grid-following (GFL) and grid-forming (GFM) inverters installed in the field for fault study and protection relay evaluation.
- Understand the GFL and GFM IBR fault responses, especially under unbalanced faults, and assess the impact of GFL and GFM IBRs on the protection relay elements with various grid operating conditions, especially when the IBRs are the only source of the fault current contribution.
- Propose and validate enhanced protection schemes to address the challenges brought by IBRs, such as the lack of negative-sequence current.

- Provide recommendations for protection scheme enhancement, including relay logic modifications, adaptive settings, or advanced protection philosophies suited for weak, IBR-dominated grids.

## 1.3 Project Summary

This project designs enhanced protection schemes for the real-world weak grid area with a high penetration of IBRs. Because the existing protection schemes were originally designed for traditional synchronous machines, first, we evaluate whether the current protection scheme will continue to operate reliably in systems with high levels of IBRs. Hardware relays are tested using a controller-hardware-in-the-loop (CHIL) setup. PSCAD electromagnetic transient (EMT) simulations with IBR original equipment manufacturer (OEM) black-box models are used to perform the fault studies and generate the COMTRADE data, which are replayed by an RTDS to feed input to the hardware relays.

Three scenarios are analyzed: normal operation, an N-1 contingency, and IBR-only scenario. The evaluation results reveal the following: (1) The protection scheme remains reliable under normal conditions and N-1 contingencies; but (2) in the IBR-only scenarios, the differential protection (87L) continues to operate reliably, whereas the local protection elements, such as distance and directional elements, fail because of the lack of regulated negative-sequence current contributed by IBRs. Enhanced protection is designed to address the challenge of the lack of negative-sequence current from IBRs, including increased restraining factors a2 and k2 to block 32Q, or using V instead of QV ORDER for ground faults, and an enhanced mho distance element with voltage and phase angle supervision for phase-to-phase faults. The efficacy of enhanced protection logic is validated and proven to work reliably. Additionally, Institute of Electrical and Electronics Engineers (IEEE) Std. 2800-2022 negative-sequence current-compliant GFL and GFM IBRs from another vendor are tested and proven to work reliably without the need for enhanced logic; therefore, this study provides valuable information to aid utilities in decision-making when faced with protection system challenges due to IBRs, either by designing enhanced protection schemes or requesting that their IBRs comply with IEEE Std. 2800-2022 to produce regulated negative-sequence current for protection relays to make the correct decisions.

# 2 Power System Model of Fault Study

The full CAPE (phasor domain software) model for the utility system with more than 10,000 buses is received from the utility, and the reduced CAPE model is obtained to include only the weak grid area of interest with high IBRs. This reduced model in CAPE is used to manually develop the PSCAD model. This chapter describes the development of the reduced-order CAPE and PSCAD model, the model validation between the full CAPE and the reduced-order CAPE, and the model validation between the reduced-order CAPE and PSCAD.

## 2.1 PSCAD Model Development

The utility provided the transmission system model in CAPE. To study the protection challenges under high penetrations of IBRs, an EMT model is required. So, the large CAPE model is reduced to a fewer buses and validated and modeled in PSCAD. A black-box model of the IBRs is integrated with the PSCAD model. The main challenges faced during the model reduction are: (1) There is no standard practice to generate the equivalent network with IBRs, thereby causing a mismatch between currents in the non-faulted phases. (2) The transformer neutral buses are floating. To resolve these challenges, extensive troubleshooting was performed with the assistance of the CAPE support team. Additionally, transformer modeling for the fault study challenges between CAPE and PSCAD is discussed in this section.

### *2.1.1 Reduced CAPE Model and Model Validation*

The full regional network model provided by the utility in the CAPE program has more than 10,000 transmission buses. To study the line protection, the model needs to represent at least one or two buses away from the lines under study. So, the size of the full network model needs to be reduced by replacing the buses, lines, and transformers that connect them with a smaller numerically equivalent network. To reduce the model in CAPE, the number of buses that need to be retained are selected manually from a one-line diagram. In the model, the retained buses are selected to be kept, and the non-selected buses are eliminated and replaced by an equivalent network. CAPE offers two network reduction techniques: (1) The conventional technique reduces the specified set of buses and develops equivalent networks with a minimum number of buses but many branches. (2) The sparsity enhanced reduction technique mathematically determines the extra buses to retain to minimize the number of equivalent branches created. It has been observed that the equivalent network created using the sparsity enhanced reduction method showed a slightly higher error than the model created from the conventional method during the validation with the full model.

Figure 1 shows the one-line diagram of the reduced model in CAPE. The conventional method created the branches (lines) between buses with a high impedance in the reduced model. These branches are not shown in Figure 1. Line 1 (L1) (between bus 10 and bus 11) and line 2 (L2) (between bus 11 and bus 12) are the interests of the study for this project. Figure 1 shows that more than two buses are included from bus 10 and 12 because of the presence of synchronous generation at bus 1 and bus 6. To validate the reduced model in CAPE, the current fault level under three-phase and phase-to-ground (SLG) faults are compared first, and then CHIL testing is performed by taking the voltages and currents for a fault on L1 and L2 and comparing the relay responses between the full and the reduced CAPE models. For simplicity, L1 and L2 are considered to be a single line, and R1 and R4 are protection relays for the combined line. Table 1 and Table 2 show the total three-phase and SLG fault current between the CAPE reduced and full

model. The fault current shows a maximum -4.86% error between the full and reduced CAPE model during three phases and the SLG faults, which is below the standard 10% error tolerance for the model validation. The fault current validates the equivalent voltage source strength created from the full network. The next step is to validate the models through the relay response.

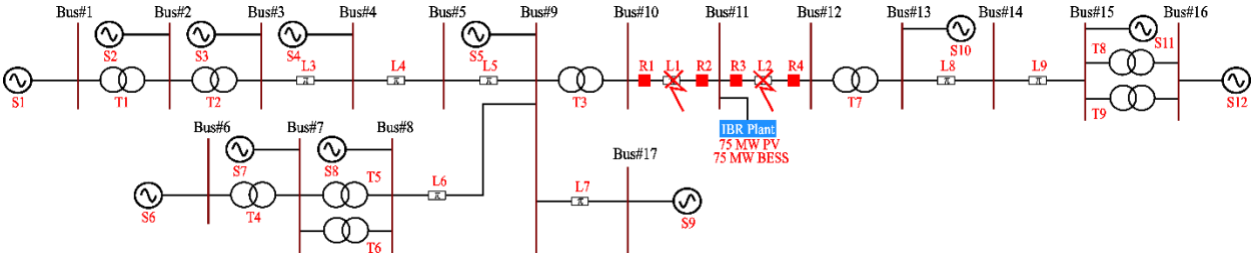


**Figure 1. One-line diagram of the reduced model**

**Table 1. Comparison of Three-Phase Fault Current Between CAPE Reduced and Full Model**

| Fault Location | Reduced Model (A) | Full Model (A) | Error |
|---|---|---|---|
| L1: 50% of line | 3989.7 | 4029.7 | -0.99% |
| L2: 50% of line | 4749.4 | 4733.9 | 0.33% |
| L8: 50% of line | 7212.7 | 7187.7 | 0.35% |
| L9: 50% of line | 13177.8 | 13107.4 | 0.54% |
| L5: 50% of line | 8247.8 | 8669.2 | -4.86% |
| L4: 50% of line | 9388.6 | 9342.7 | 0.49% |
| L3: 50% of line | 10691.8 | 10987.6 | -2.69% |

**Table 2. Comparison of SLG Fault Current Between CAPE Reduced and Full Model**

| Fault Location | Reduced Model (A) | Full Model (A) | Error |
|---|---|---|---|
| L1: 50% of line | 2641.7 | 2636.4 | 0.20% |
| L2: 50% of line | 3685.5 | 3681.5 | 0.33% |
| L8: 50% of line | 6849.5 | 6833.8 | 0.35% |
| L9: 50% of line | 10453.9 | 10427.7 | 0.54% |
| L5: 50% of line | 7135.5 | 7383.7 | -4.86% |
| L4: 50% of line | 8271.1 | 8594.4 | 0.49% |
| L3: 50% of line | 9564.4 | 9887.6 | -2.69% |

Three unbalanced faults, phase-to-ground, phase-to-phase, and phase-to-phase-to-ground, are simulated in CHIL to compare the relay responses between the full and reduced CAPE model. Figure 2 shows the relay (R1) response between the full and reduced model. Traces in red and labels starting with 1 are from the full model. Blue traces and labels starting with 2 are from the reduced model. The red and blue traces closely match, which validates the accuracy of the red model. The impedance ZAG traces for the full and reduced model converge to the same point for the SLG fault. Digital bits show that the differential and impedance elements assert at approximately the same time. A similar explanation is applicable to Figure 3–Figure 7; however, Figure 4 and Figure 5 show that the Z1P and Z2P digital bits assert faster than the reduced model response. The relay response with reduced model is slightly slower because the rise in the fault current is slightly less than the full model, thereby delaying the current threshold in the phase impedance element (Z1P, Z2P) to assert. This delay is acceptable because the delay from Table 3 is 2 ms, which is less than one-quarter (4.16 ms) of a cycle.

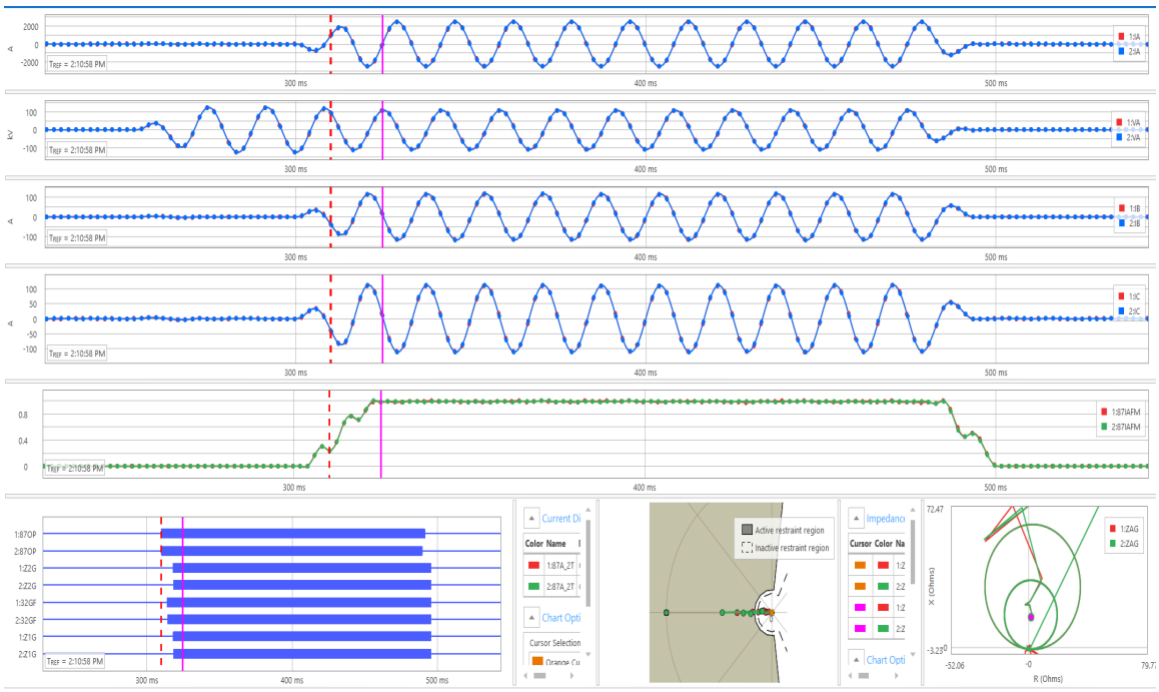

**Figure 2. R1 response for an SLG fault between bus 10 and bus 12 at 25% of the fault locations**

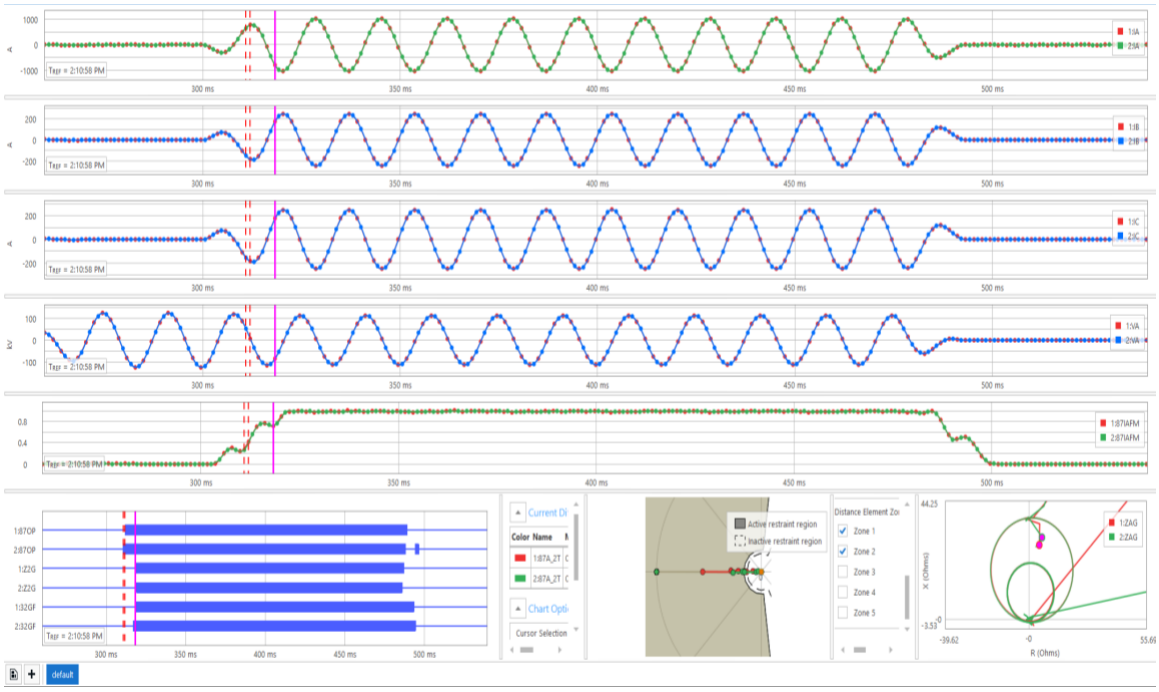

**Figure 3. R4 response for an SLG fault between bus 10 and bus 12 at 25% of the fault locations from bus 10**

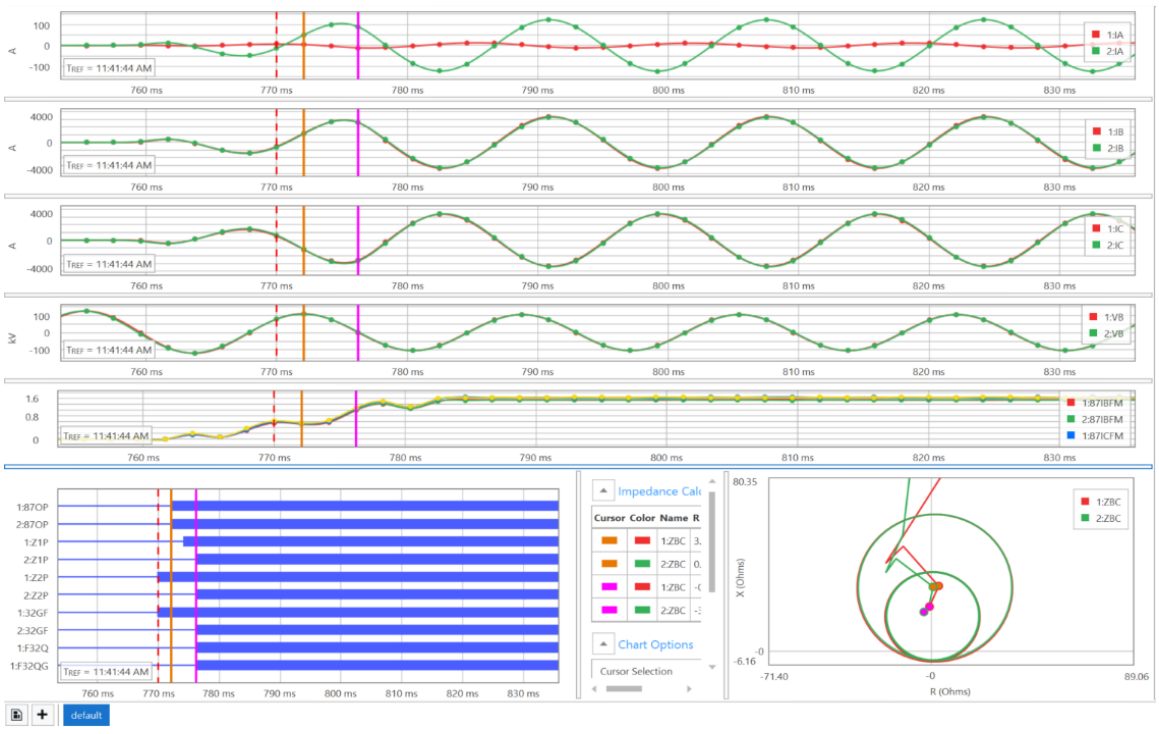

**Figure 4. R1 response for a phase-to-phase fault between bus 10 and bus 12 at 25% of the fault locations**

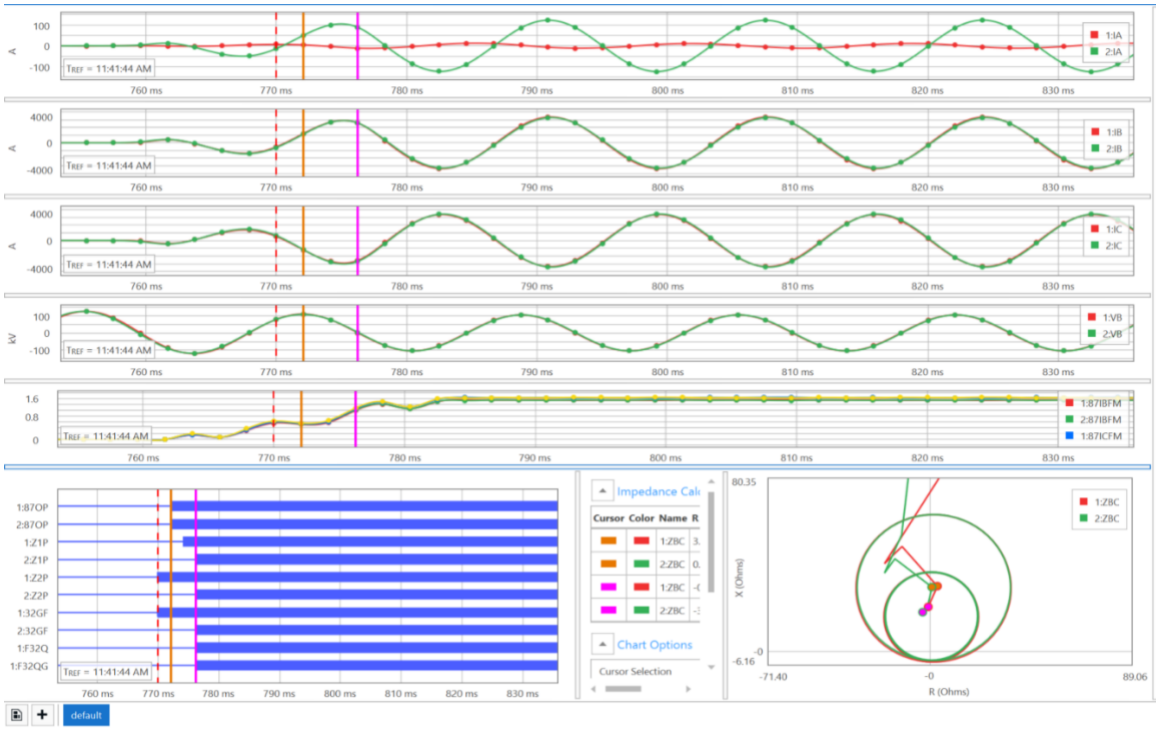


**Figure 5. R4 response for a phase-to-phase fault between bus 10 and bus 12 at 25% of the fault locations**

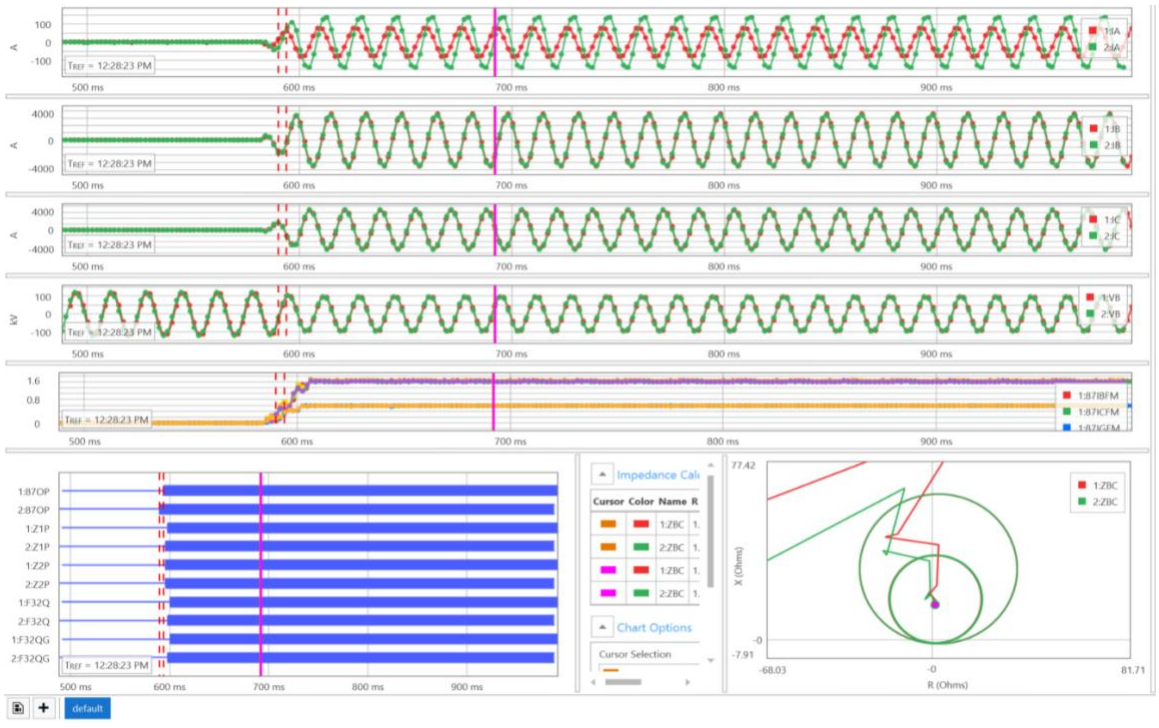


**Figure 6. R1 response for a phase-to-phase-to-ground fault between bus 10 and bus 12 at 25% of the fault locations**

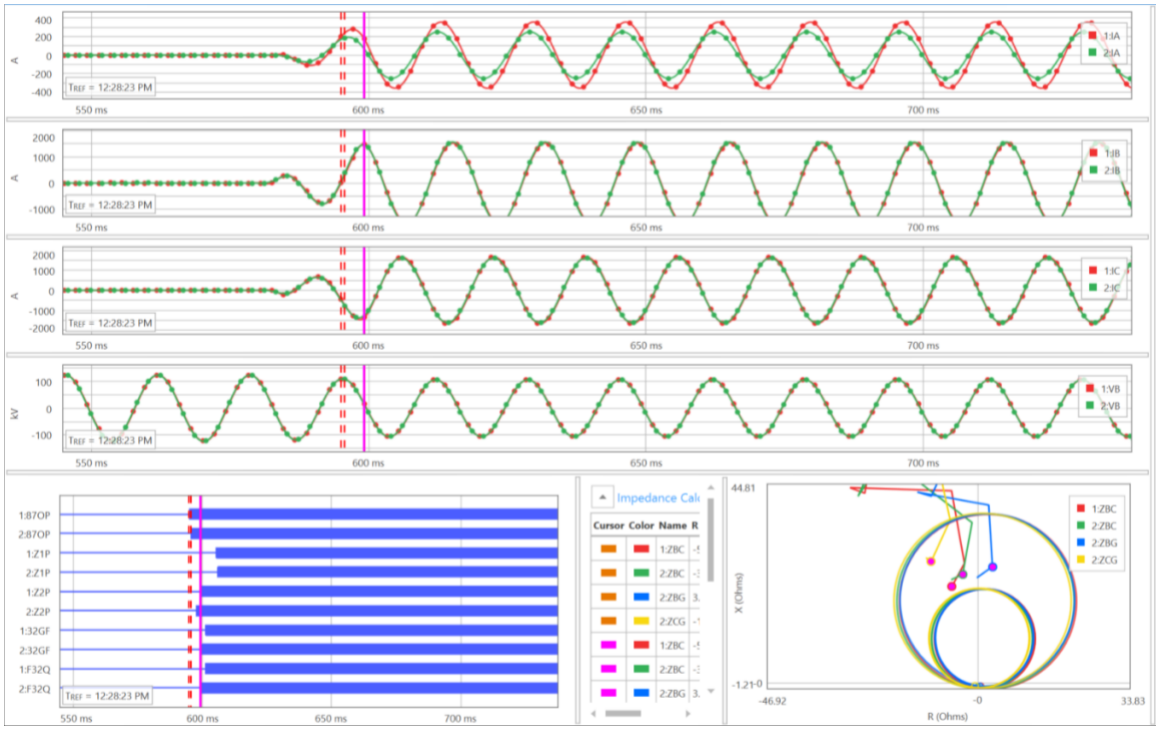

**Figure 7. R4 response for a phase-to-phase-to-ground fault between bus 10 and bus 12 at 25% of the fault locations**

Table 3 shows the R1, R4 distance element response summary for an SLG fault, a phase-to-phase fault, and a phase-to-phase-to-ground fault. The differential and distance element pickup time are compared between the full and reduced model. Table 3 shows the maximum pickup time difference of 3 ms for the phase-to-phase-to-ground fault and the differential element. Because the maximum difference is less than one-quarter of a cycle (~4 ms), the reduced model is an accurate representation of the full network model. Also, the fault location calculated by the relay for the full and reduced model is almost the same, therefore further validating the accuracy of the reduced model.

**Table 3. Comparison of Relay Responses for the Same Fault Applied to the CAPE Full Model and the CAPE Reduced Model**

| Fault Type | Relay | 87OP Time Diff. | Z1P/Z1G Time Diff. | Z2P/Z2G Time Diff. | Fault Location | |
|---|---|---|---|---|---|---|
| | | | | | Full Model | Reduced Model |
| AG | R1 | No diff. | No diff. | No diff. | 51.7 mi | 51.49 mi |
| | R4 | 1 ms | N/A | 1 ms | 153.35 mi | 152.97 mi |
| BC | R1 | No diff. | 2 ms | 1.3 ms | 50.53 mi | 50.53 mi |
| | R4 | No diff. | 2 ms | No diff. | 115.81 mi | 115.61 mi |
| BCG | R1 | 3 ms | 1.8 ms | 0.2 ms | 50.57 mi | 50.52 mi |
| | R4 | 0.6 ms | 0.6 ms | 1.4 ms | 115.67 mi | 114.82 mi |

### 2.1.2 PSCAD Model and Model Validation

Converting the phasor domain model to EMT requires a careful transition of network parameters for accurate representation. Voltage sources are modeled in sequence impedances, which can be used directly in the PSCAD source model. Lines are also modeled using positive-, negative-, and zero-sequence impedances in CAPE. In PSCAD, the PI model is used to represent the lines, and CAPE sequence parameters are directly used in the PI model. There are nine transformers, including two-winding and three-winding transformers, in the CAPE reduced model. T2, T3, T5, T6, T7, T8, and T9 are the three-winding auto transformers, and T1 and T4 are the two-winding transformers. The transformers are the ground sources for the ground faults, depending on the neutral connection. It is crucial to accurately model the transformer because the positive, negative, and zero sequence of the transformer can affect the fault impedance network. In CAPE, transformers are modeled using positive-, negative-, and zero-sequence impedances; however, the PSCAD standard library transformers require only positive-sequence leakage reactance for the transformer modeling. In the PSCAD library, all the transformers are three-limb core type, and there is no provision to change the zero-sequence impedance. To match the SLG fault currents, a transformer model with a zero-sequence parameter is required; therefore, a custom transformer model from PSCAD is used to represent the two-winding and three-winding transformers. Subsections 2.1.2.1 and 2.1.2.2 explain the procedure to convert the CAPE transformer sequence parameters to the PSCAD custom transformer model parameters. The leakage reactance parameters for these transformers are derived from the CAPE model by isolating lines and created the single source for the SLG ground fault sequence data at the transformer terminals.

#### 2.1.2.1 Two-Winding Transformer Zero-Sequence Impedance

Figure 8 (a) shows the SLG sequence network of a two-winding transformer with a single source. $Z1_{source}$, $Z2_{source}$, and $Z0_{source}$ are the positive-, negative-, and zero-sequence impedances of the source, respectively. $Z1_{transformer}$, $Z2_{transformer}$, $Z0_{transformer}$, $Z1_{line}$, $Z2_{line}$, and $Z0_{line}$ are the positive-, negative-, and zero-sequence impedances of the transformer and line, respectively. This transformer sequence network is for delta-wye grounded transformers because the two-winding transformers in the reduced model are of a similar configuration. A similar procedure can be applied to other transformer configurations with a neutral grounding.

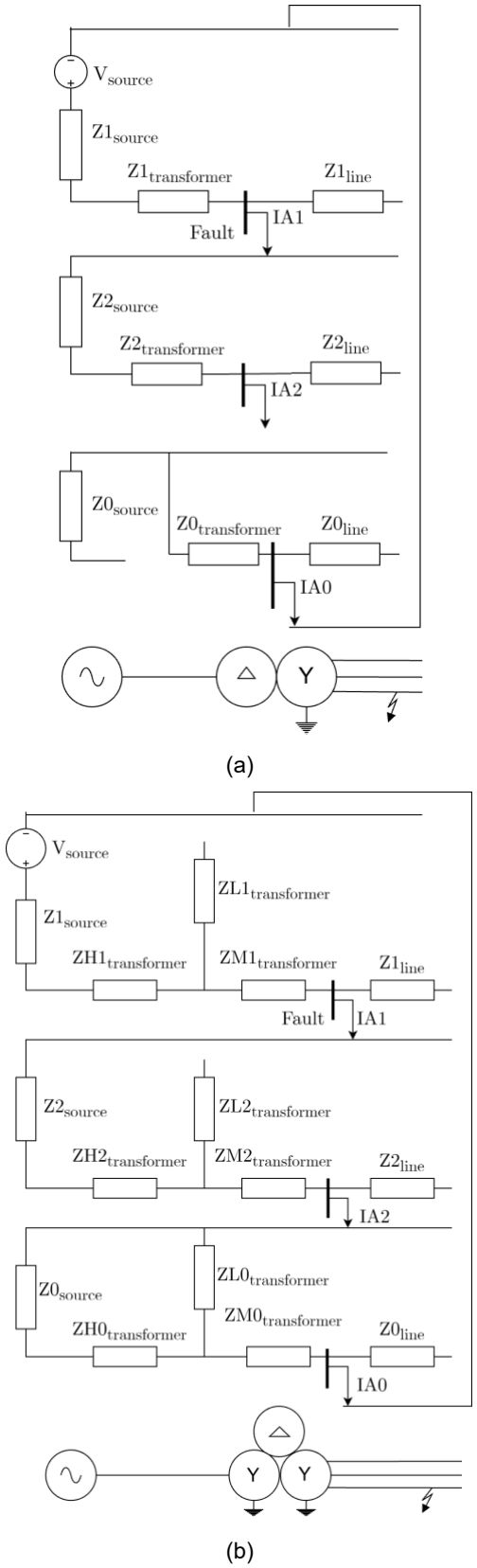


**Figure 8. Sequence diagrams of (a) two-winding and (b) three-winding transformer SLG faults [1]**

To derive the zero-sequence impedance of the respective two-winding transformers, a simple circuit with one voltage source is created by isolating the necessary lines, voltage sources, and transformers. An SLG fault is placed on the high side of a transformer to include the neutral grounding. From the sequence network, phase current IA can be calculated using Eq. 1. Sequence currents are calculated using Eq. 2. Finally, the zero-sequence transformer impedance is calculated using Eq. 3. Then we calculate the zero-sequence over the positive-sequence transformer ratio as an input to the transformer parameters, as shown in Figure 9.

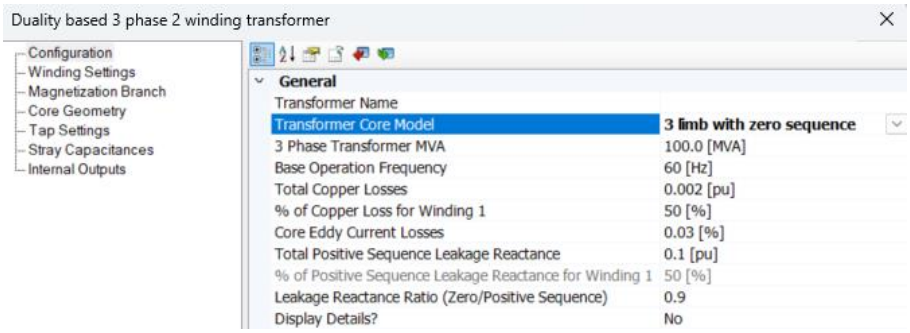


**Figure 9. Custom two-winding transformer model with zero-sequence impedance**

$$IA = 3\text{IA1} = 3\text{IA2} = 3\text{IA0} \tag{1}$$

$$IA1 = \text{IA2} = \text{IA0} = \frac{V_{source}}{Z1_{transformer} + Z2_{transformer} + Z0_{transformer}} \tag{2}$$

$$Z0_{transformer} = \left(3V_{source}/_{IA}\right) - Z1_{transformer} - Z2_{transformer} \tag{3}$$

### 2.1.2.2 Three-Winding Transformer Zero-Sequence Impedance

Three-winding transformers present several challenges due to the inherent complexity in modeling. These transformers are modeled using leakage impedances between windings (1–2, 1–3, 2–3), as shown in Figure 10. $ZH1_{transformer}$, $ZH2_{transformer}$, $ZH0_{transformer}$, $ZM1_{transformer}$, $ZM2_{transformer}$, $ZM0_{transformer}$, $ZL1_{transformer}$, $ZL2_{transformer}$, and $ZL0_{transformer}$ are the positive-, negative-, and zero-sequence impedances of the high-, medium-, and low-voltage network, respectively. For fault studies, these impedances are converted to an equivalent wye type or T network. This equivalent wye or T is a mathematical representation to determine the currents and voltages at the transformer terminals. The neutral point in the equivalent wye or T has no physical meaning.

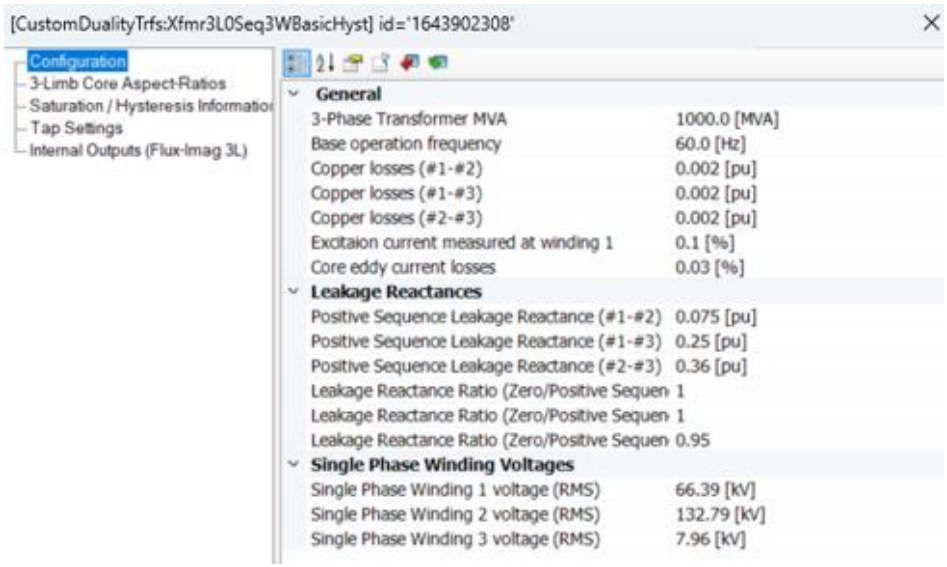


**Figure 10. Custom three-winding transformer parameters**

To convert the CAPE parameters to PSCAD, the first step is to calculate the equivalent wye or T network. Figure 8 (b) shows the sequence network of a three-winding transformer with a wye or T network for an SLG fault on the high side of a transformer with a single source. ZH, ZM, and ZL in Figure 8 (b) form the T network. The next step is to aggregate the positive-, negative-, and zero-sequence impedances of the network from Figure 8 (b). Eqs. 4, 5, and 6 show the aggregated impedances of the network in Figure 8 (b). From Eqs. 1, 2, and 3, the aggregated Z0 can be calculated. From CAPE, $ZH0_{transformer}$ is calculated from the CAPE transformer parameters. Because the other zero-sequence parameters in the T network are not known, we assume one of the parameters to be 85%–100% of the positive-sequence values, and we calculate the other unknown zero-sequence parameter:

$$Z1 = \mathrm{Z1}_{source} + ZH1_{transformer} + ZM1_{transformer} \quad (4)$$

$$Z2 = \mathrm{Z2}_{source} + ZH2_{transformer} + ZM2_{transformer} \quad (5)$$

$$Z0 = ((\mathrm{Z0}_{source} + ZH0_{transformer})//ZL0_{transformer}) + ZM0_{transformer} \quad (6)$$

### 2.1.2.3 PSCAD Model Validation

All the components in CAPE are converted to PSCAD parameters, and the network model is developed. It is crucial to extensively validate the PSCAD model against the CAPE model to perform protection studies. A balanced and unbalanced fault are simulated at various locations to compare the fault currents from equivalent voltage sources and lines. Table 4, Table 6, and Table 8 show the three-phase fault current comparisons between CAPE and PSCAD at the buses and transmission lines. The maximum error between the CAPE and PSCAD fault currents is 10%. Because the error is within the standard limits (≤10%), the PSCAD model for three-phase faults

is an accurate representation of the CAPE model. With unbalanced faults such as an SLG, the zero-sequence network is validated, thereby the overall network model can be validated. Table 5, Table 7, and Table 9 show the comparison of the phase and zero-sequence fault currents for the SLG. The maximum error occurs in the zero-sequence currents (highlighted in red in each table), which exceeds the standard error limit (≤10%). When the small-magnitude numbers are compared, the relative error is high, but the absolute error is small. This error is acceptable because the zero-sequence current magnitudes are less than 20 A.

**Table 4. Comparison of the CAPE Reduced and PSCAD Model for a Three-Phase Fault on Bus 10**

| Voltage Sources | Current (kA) | | Error |
|---|---|---|---|
| | CAPE | PSCAD | |
| Bus 2 | 0.147 | 0.162 | -10% |
| Bus 3 | 1.54 | 1.38 | 10% |
| Bus 6 | 4.634 | 4.436 | 4% |
| Bus 7 | 0.445 | 0.488 | -10% |
| Bus 8 | 1.157 | 1.105 | 4% |
| Bus 4 | 0.378 | 0.385 | -2% |
| Bus 9 | 2.078 | 2.142 | -3% |
| Bus 13 | 0.107 | 0.099 | 7% |
| Bus 15 | 0.303 | 0.307 | -1% |
| Bus 16 | 0.117 | 0.1135 | 3% |
| **Transmission Lines** | | | |
| L3 | 1.384 | 1.49 | -8% |
| L4 | 1.76 | 1.864 | -6% |
| L5 | 1.76 | 1.86 | -6% |
| L1 | 0.944 | 0.967 | -2% |
| L2 | 0.944 | 0.967 | -2% |
| L6 | 2.563 | 2.617 | -2% |
| **Total Fault Current** | **10.545** | **10.162** | **4%** |

**Table 5. Comparison of the CAPE Reduced and PSCAD Model for an SLG Fault on Bus 10**

| Voltage Sources | Current (kA) | | | Zero-Sequence Current (kA) | | |
|---|---|---|---|---|---|---|
| | CAPE | PSCAD | Error | CAPE | PSCAD | Error |
| Bus 2 | 0.109 | 0.12 | -10% | 0.0082 | 0.0086 | -5% |
| Bus 3 | 1.143 | 1.15 | -1% | 0.079 | 0.072 | 9% |
| Bus 6 | 3.322 | 3.317 | 0% | 0.0001 | 0.0001 | 0% |
| Bus 7 | 0.37 | 0.4 | -8% | 0.008 | 0.008 | 0% |
| Bus 8 | 1.078 | 1.052 | 2% | 0.138 | 0.129 | 7% |
| Bus 4 | 0.38 | 0.391 | -3% | 0.09 | 0.085 | 6% |
| Bus 9 | 2.7 | 2.66 | 1% | 1.02 | 0.975 | 4% |
| Bus 13 | 0.097 | 0.088 | 9% | 0.0113 | 0.0126 | -12% |
| Bus 15 | 0.247 | 0.244 | 1% | 0.0013 | 0.0014 | -8% |
| Bus 16 | 0.095 | 0.097 | -2% | 0.00063 | 0.00068 | -8% |
| **Transmission Lines** | | | | | | |
| L3 | 1.27 | 1.25 | 2% | 0.1 | 0.094 | 6% |
| L4 | 1.672 | 1.64 | 2% | 0.188 | 0.176 | 6% |
| L5 | 1.672 | 1.64 | 2% | 0.188 | 0.176 | 6% |
| L1 | 0.815 | 0.831 | -2% | 0.057 | 0.062 | -9% |
| L2 | 0.815 | 0.831 | -2% | 0.057 | 0.062 | -9% |
| L6 | 2.29 | 2.28 | 0% | 0.214 | 0.205 | 4% |
| **Total Fault Current** | **12.37** | **11.85** | **4%** | | | |

**Table 6. Comparison of the CAPE Reduced and PSCAD Model for a Three-Phase Fault on Bus 9**

| Voltage Sources | Current (kA) | | Error |
|---|---|---|---|
| | CAPE | PSCAD | |
| Bus 2 | 0.163 | 0.171 | -5% |
| Bus 3 | 1.709 | 1.705 | 0% |
| Bus 6 | 5.985 | 5.461 | 9% |
| Bus 7 | 0.575 | 0.613 | -7% |
| Bus 8 | 1.495 | 1.479 | 1% |
| Bus 4 | 0.464 | 0.482 | -4% |
| Bus 9 | 2.684 | 2.708 | -1% |
| Bus 13 | 0.105 | 0.097 | 8% |
| Bus 15 | 0.296 | 0.302 | -2% |
| Bus 16 | 0.114 | 0.111 | 3% |
| **Transmission Lines** | | | |
| L3 | 1.891 | 1.884 | 0% |
| L4 | 2.355 | 2.349 | 0% |
| L5 | 2.355 | 2.36 | 0% |
| L1 | 0.923 | 0.932 | -1% |
| L2 | 0.922 | 0.932 | -1% |
| L6 | 3.311 | 3.311 | 0% |
| **Total Fault Current** | **8.998** | **8.976** | **0%** |

**Table 7. Comparison of the CAPE Reduced and PSCAD Model for an SLG Fault on Bus 9**

| Voltage Sources | Current (kA) | | | Zero-Sequence Current (kA) | | |
|---|---|---|---|---|---|---|
| | CAPE | PSCAD | Error | CAPE | PSCAD | Error |
| Bus 2 | 0.135 | 0.145 | -7% | 0.0123 | 0.013 | -6% |
| Bus 3 | 1.415 | 1.418 | 0% | 0.1203 | 0.11 | 9% |
| Bus 6 | 3.997 | 3.813 | 5% | 0.0001 | 0.0001 | 0% |
| Bus 7 | 0.448 | 0.487 | -9% | 0.012 | 0.011 | 8% |
| Bus 8 | 1.343 | 1.335 | 1% | 0.208 | 0.191 | 8% |
| Bus 4 | 0.488 | 0.502 | -3% | 0.135 | 0.122 | 10% |
| Bus 9 | 3.573 | 3.533 | 1% | 1.542 | 1.426 | 8% |
| Bus 13 | 0.09 | 0.084 | 7% | 0.011 | 0.011 | 0% |
| Bus 15 | 0.226 | 0.223 | 1% | 0.00123 | 0.00138 | -12% |
| Bus 16 | 0.087 | 0.095 | -9% | 0.0006 | 0.00065 | -8% |
| **Transmission Lines** | | | | | | |
| L3 | 1.584 | 1.25 | 21% | 0.151 | 0.136 | 10% |
| L4 | 2.072 | 1.64 | 21% | 0.285 | 0.259 | 9% |
| L5 | 2.073 | 1.64 | 21% | 0.285 | 0.259 | 9% |
| L1 | 0.756 | 0.831 | -10% | 0.055 | 0.056 | -2% |
| L2 | 0.756 | 0.831 | -10% | 0.055 | 0.056 | -2% |
| L6 | 2.837 | 2.28 | 20% | 0.325 | 0.3 | 8% |
| **Total Fault Current** | **10.243** | **10.374** | **-1%** | | | |

**Table 8. Comparison of the CAPE Reduced and PSCAD Model for a Three-Phase Fault on Line L1 at the 15% Fault Location**

| Voltage Sources | Current (kA) | | Error |
|---|---|---|---|
| | CAPE | PSCAD | |
| Bus 2 | 0.069 | 0.074 | -7% |
| Bus 3 | 0.724 | 0.74 | -2% |
| Bus 6 | 2.529 | 2.612 | -3% |
| Bus 7 | 0.263 | 0.285 | -8% |
| Bus 8 | 0.632 | 0.646 | -2% |
| Bus 4 | 0.196 | 0.215 | -10% |
| Bus 9 | 1.134 | 1.176 | -4% |
| Bus 13 | 0.117 | 0.11 | 6% |
| Bus 15 | 0.329 | 0.347 | -5% |
| Bus 16 | 0.127 | 0.121 | 5% |
| **Transmission Lines** | | | |
| L3 | 0.8 | 0.798 | 0% |
| L4 | 0.995 | 1.018 | -2% |
| L5 | 0.995 | 1.018 | -2% |
| L1 | 5.041 | 5.02 | 0% |
| L2 | 1.032 | 1.042 | -1% |
| L6 | 1.4 | 1.43 | -2% |
| **Total Fault Current** | **6.074** | **6.049** | **0%** |

**Table 9. Comparison of the CAPE Reduced and PSCAD Model for an SLG Fault on Line L1 at the 15% Fault Location**

| Voltage Sources | Current (kA) | | | Zero-Sequence Current (kA) | | |
|---|---|---|---|---|---|---|
| | CAPE | PSCAD | Error | CAPE | PSCAD | Error |
| Bus 2 | 0.037 | 0.04 | -8% | 0.003 | 0.0028 | 7% |
| Bus 3 | 0.388 | 0.398 | -3% | 0.028 | 0.0253 | 10% |
| Bus 6 | 1.1 | 1.17 | -6% | 0.0001 | 0.0001 | 0% |
| Bus 7 | 0.138 | 0.15 | -9% | 0.0026 | 0.0024 | 8% |
| Bus 8 | 0.358 | 0.39 | -9% | 0.045 | 0.045 | 0% |
| Bus 4 | 0.13 | 0.14 | -8% | 0.0326 | 0.0296 | 9% |
| Bus 9 | 0.894 | 0.925 | -3% | 0.3329 | 0.338 | -2% |
| Bus 13 | 0.09 | 0.084 | 7% | 0.0328 | 0.0333 | -2% |
| Bus 15 | 0.167 | 0.154 | 8% | 0.0067 | 0.007 | -4% |
| Bus 16 | 0.074 | 0.081 | -9% | 0.0018 | 0.002 | -11% |
| **Transmission Lines** | | | | | | |
| L3 | 0.433 | 0.43 | 1% | 0.036 | 0.033 | 8% |
| L4 | 0.563 | 0.57 | -1% | 0.068 | 0.062 | 9% |
| L5 | 0.563 | 0.57 | -1% | 0.068 | 0.062 | 9% |
| L1 | 3.841 | 3.776 | 2% | 1.34 | 1.32 | 1% |
| L2 | 0.678 | 0.7 | -3% | 0.165 | 0.167 | -1% |
| L6 | 0.764 | 0.87 | -14% | 0.07 | 0.071 | -1% |
| **Total Fault Current** | **4.52** | **4.458** | **1%** | | | |

The next step in the validation is to study the relay response when the voltages and currents from CAPE and PSCAD are run through the CHIL setup. Figure 11 and Figure 12 show the R1 and R4 responses for a close-in fault on L1. Traces in red are from CAPE, whereas green traces are from PSCAD. Fault pickup and trip elements are represented using the digital plots. The mho element trajectory between the CAPE and PSCAD models is different because the pre-fault current is different between the models. Because there are no loads in the model, the pre-fault current in each model depends on the voltages and phase angles at each bus. So, the load impedance (V/I) is different, and therefore their trajectories are different, but both models show similar fault impedances. Compared to the CAPE data, the differential element operated 1 ms slower with the PSCAD data. Zone 2 elements from the PSCAD data operated slightly faster but were still less than one-quarter of a cycle.


**Figure 11. R1 response of the CAPE and PSCAD model for a three-phase close-in fault on bus 10**

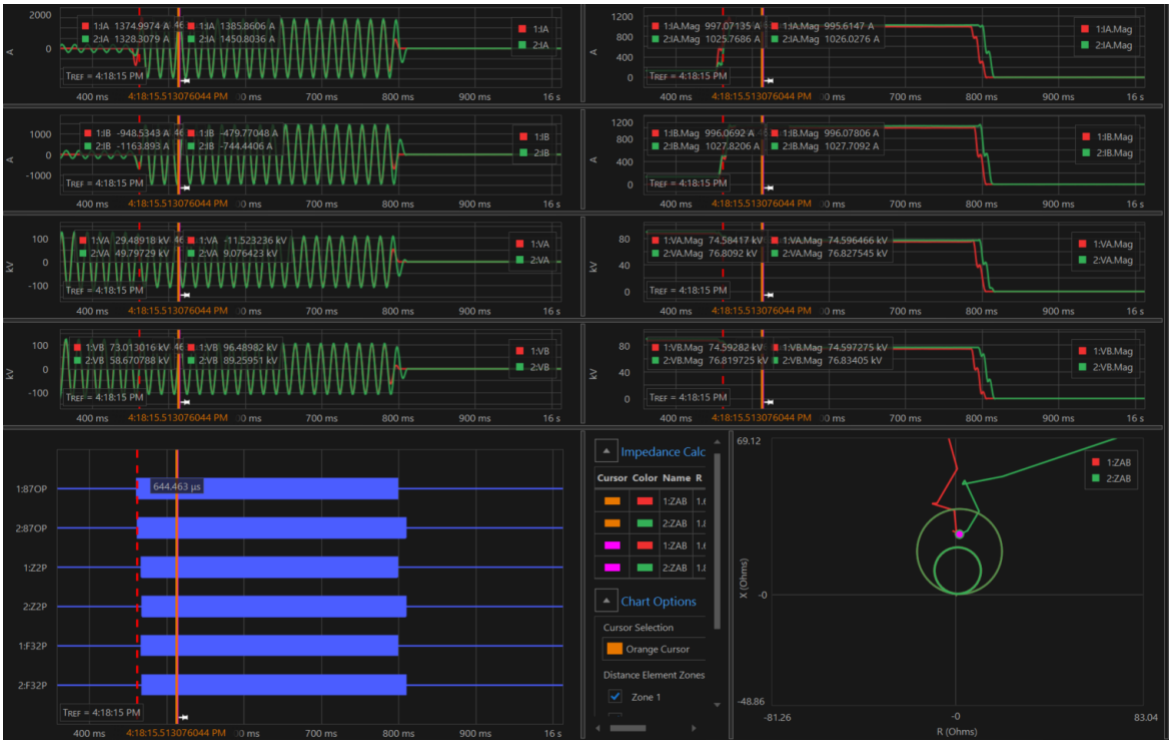


**Figure 12. R4 response of the CAPE and PSCAD model for a three-phase close-in fault on bus 10**

Figure 13 and Figure 14 show the R1, R4 response for an SLG fault on L1. The differential elements and zone 2 distance elements operated faster, approximately 1 ms, for the PSCAD model. Because the difference is 1 ms, it can be assumed that both models operated at the same time.


**Figure 13. R1 response of the CAPE and PSCAD model for an SLG close-in fault on bus 10**


**Figure 14. R4 response of the CAPE and PSCAD model for an SLG close-in fault on bus 10**

Table 10 provides a summary of the differential element and distance element operation for three-phase and SLG faults on L1. For both faults, the PSCAD model relay response is slightly faster, approximately 1 ms, except for the three-phase fault distance elements at 3.2 ms (less than one-quarter of a cycle). Both the fault location and protection elements are within acceptable limits. Because the time difference of the differential and distance elements between the CAPE and PSCAD model for various faults is less than one-quarter of a cycle, the PSCAD model is an accurate representation for fault studies.

**Table 10. Comparison of the Relay Response to the Same Fault Applied to the CAPE Reduced Model and the PSCAD Reduced Model**

| Fault Type | Relay | 87OP Time Diff. | Zone Element Time Diff. | Fault Location | |
|---|---|---|---|---|---|
| | | | | CAPE | PSCAD |
| AG | R1 | 0.7 ms | 1.2 ms | 5.21 mi | 5.23 mi |
| | R4 | 1.0 ms | 1.1 ms | 155.27 mi | 154.69 mi |
| ABCG | R1 | 1.0 ms | 3.2 ms | 5.06 mi | 5.06 mi |
| | R4 | 0.7 ms | 0.7 ms | 152.59 mi | 152.39 mi |

## 2.2 Black-Box GFL and GFM Inverter Model

Two distinct types of IBRs were analyzed, both rated at 75 MVA: a GFL inverter representing a PV plant and a GFM inverter representing a battery energy storage system. The inverter vendor provided these models as OEM black-box units. This means that the models accurately represent

the physical IBRs in the field, including proprietary and confidential internal control logic. Using these black-box models is essential for an accurate protection study, as the control response of the inverter dictates its fault characteristics. These models were integrated into the PSCAD simulation environment. Unlike phasor-based tools, such as the current injection model (CAPE), an EMT program, such as PSCAD, is required to capture the fast, sub-cycle, and often nonlinear dynamics of IBRs during a fault.

### 2.2.1 Fault Response of GFL and GFM IBRs

To understand the fault characteristics, an unbalanced (BC) fault was applied to the system. The resulting current injection from the GFL and GFM inverters was analyzed using symmetrical components (shown in Figure 15) with active component of positive sequence current, $I1A \coloneqq |I1|\cos(\angle V1 - \angle I1)$; reactive component of the positive sequence current, $I1R \coloneqq |I1|\sin(\angle V1 - \angle I1)$; active component of negative sequence current, $I2A \coloneqq |I2|\cos(\angle V2 - \angle I2)$; reactive component of the negative sequence current, $I2R \coloneqq |I2|\sin(\angle V2 - \angle I2)$ [2]. This is critically important because traditional transmission line protection elements (such as mho distance, 32P, and 32Q) fundamentally rely on the presence of negative sequence current with the consistent phase relationship between negative sequence current and negative sequence voltage ($I_2$ leads $V_2$ by approximately 90°) to detect and determine the direction of unbalanced faults. Note that the GFM IBR doesn't generate regulated negative sequence current either.

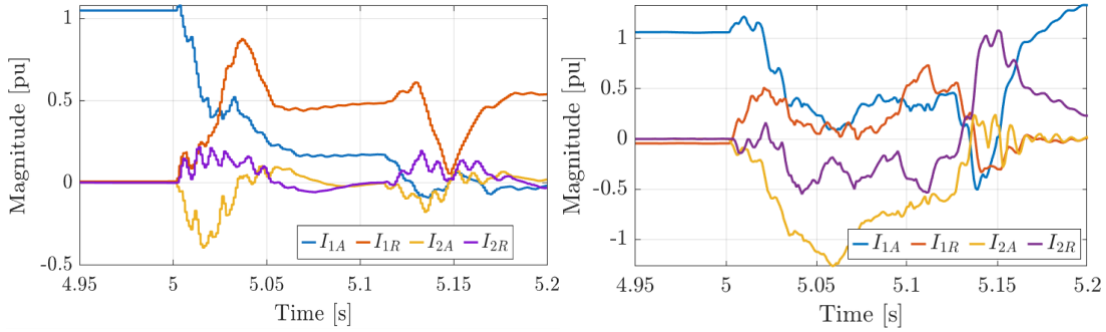


**Figure 15. GFL (left) and GFM (right) inverter fault current responses under a BC fault**

### 2.2.2 Findings and Implications

IEEE Std. 2800-2022 provides a modern framework for IBR fault responses [3]. When supporting the grid, ideally, a compliant inverter would inject negative-sequence current in a way that helps the protection scheme (e.g., negative-sequence current leading the negative-sequence voltage by 90°, resulting in $I2A \approx 0$ and $I2R \approx -|I2|$). But the fault response plot (shown in Figure 15) for the GFL and GFM models reveals two major issues: (1) Both the GFL and GFM IBRs do not comply with the IEEE Std. 2800-2022 negative-sequence current requirement. They fail to provide a stable negative-sequence current that traditional relays are designed to detect, and the negative-sequence current does not lead the negative-sequence voltage by 90°. (2) The fault currents are oscillatory and have low magnitudes. These findings pose challenges to traditional protection schemes. The low-fault-current contribution challenges the sensitivity of traditional protection; overcurrent and distance elements might not identify the fault and fail to operate. The lack of negative-sequence current mis-operates the directional and fault dentification elements, rendering them unreliable. These nonstandard fault characteristics pose significant challenges to the reliability of protection schemes, particularly in IBR-only scenarios.

# 3 Framework of the Protection System Study

This chapter presents the protection study methodology, the use case study, and the laboratory CHIL evaluation setup.

## 3.1 Protection Study Methodology

Figure 16 shows the schematic diagram of the proposed protection study methodology. First, we have the PSCAD model ready with the integrated OEM GFL black-box model. Three scenarios are considered: the normal condition, the N-1 contingency, and the IBR-only scenarios. The PSCAD model is used to run the fault studies with all the considered scenarios, and the COMTRADE data from the PSCAD simulation is saved and replayed in the RTDS. The hardware relays are connected to the RTDS through inputs/outputs and fiber-optics; and the relay settings, the current transformer/potential transformer ratios, etc., are validated through multiple field event data. An automatic script is developed to run all the fault scenarios and evaluate the relay responses. Then, we identify the protection issues and make suggestions to enhance and improve the protection system reliability and security [4].

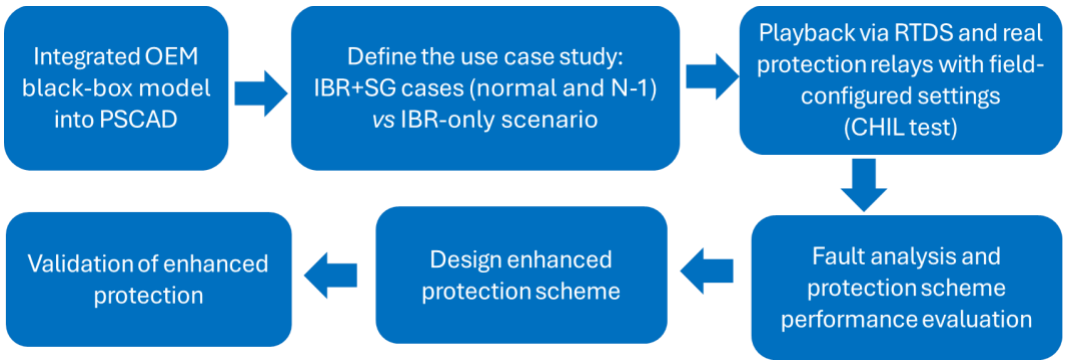


**Figure 16. Schematic diagram of the protection study methodology [4]**

## 3.2 Use Case Study

A comprehensive set of use case studies was created to assess the performance of the existing relay protection schemes. These studies aimed to evaluate the relay response across a diverse range of fault conditions and system topologies, with a particular emphasis on identifying issues that emerge in scenarios with high IBR penetrations. The testing matrix concentrates on the two main transmission line sections of interest: L1 and L2. A matrix comprising more than 100 test scenarios was developed to simulate a broad spectrum of realistic events. Each scenario was characterized by a combination of factors, as outlined in Table 11. All the contingency scenarios are grouped under three subcategories: normal (gray shading), N-1 contingency (blue shading), and IBR-only source (red text). When L2 is out of service, it creates a condition in which the IBR is the only source, and therefore it is classified as IBR-only to differentiate from other N-1 contingencies. Protection studies are primarily focused on three faults: phase-to-ground faults, phase-to-phase faults, and phase-to-phase-to-ground faults. Three fault locations are considered: close-in from L1 (5%), end of zone 1 from L1 (80%), and remote close-in from L1 (95%). For L2, the contingency scenarios are the same except that in the IBR case, L1 is out of service, as outlined in Table 12.

**Table 11. Test Scenario Design for L1**

| Contingency | 5% of L1 | | | 80% of L1 | | | 95% of L1 | | |
|---|---|---|---|---|---|---|---|---|---|
| | AG | BC | BCG | AG | BC | BCG | AG | BC | BCG |
| All in service | ✓ | ✓ | ✓ | ✓ | ✓ | ✓ | ✓ | ✓ | ✓ |
| S5 | ✓ | ✓ | ✓ | ✓ | ✓ | ✓ | ✓ | ✓ | ✓ |
| S10 | ✓ | ✓ | ✓ | ✓ | ✓ | ✓ | ✓ | ✓ | ✓ |
| L5 | ✓ | ✓ | ✓ | ✓ | ✓ | ✓ | ✓ | ✓ | ✓ |
| L6 | ✓ | ✓ | ✓ | ✓ | ✓ | ✓ | ✓ | ✓ | ✓ |
| L8 | ✓ | ✓ | ✓ | ✓ | ✓ | ✓ | ✓ | ✓ | ✓ |
| L2 | ✓ | ✓ | ✓ | ✓ | ✓ | ✓ | ✓ | ✓ | ✓ |

**Table 12. Test Scenario Design for L2**

| Contingency | 5% of L2 | | | 80% of L2 | | | 95% of L2 | | |
|---|---|---|---|---|---|---|---|---|---|
| | AG | BC | BCG | AG | BC | BCG | AG | BC | BCG |
| All in service | ✓ | ✓ | | ✓ | | | ✓ | ✓ | |
| S5 | ✓ | ✓ | | | | | | | |
| S10 | ✓ | ✓ | | | | | | | |
| L5 | ✓ | ✓ | | | | | | | |
| L6 | ✓ | ✓ | | | | | | | |
| L8 | ✓ | ✓ | | | | | | | |
| L1 | ✓ | ✓ | ✓ | ✓ | ✓ | ✓ | ✓ | ✓ | ✓ |

### 3.2.1 Test Scenario Distribution

In total, 106 test scenarios were evaluated, as shown in Figure 17. This test suite was designed to provide extensive coverage of the system's operation conditions and fault-based behavior. The distribution of these tests is as follows:

- Contingency type: The scenarios were heavily focused on severe grid conditions—normal: 16 scenarios, N-1: 24 scenarios, IBR only: 66 scenarios.
- Fault type: The cases were well distributed among fault types, including 40 AG (phase-to-ground), 41 BC (phase-to-phase), and 25 BCG (phase-to-phase-to-ground) faults.
- Fault location: To test different protection zones, faults were applied at various locations—52 cases at 5% (close in), 24 cases at 80% (zone 2), and 30 cases at 95% (remote close in) of the line length. All distances were measured from the bus 10 for L1 and from bus 12 for L2, both toward bus 11.
- IBR power reference: Tests were run at two different IBR active power reference levels to check the influence of the IBR loading: 84 scenarios at a very light load (0.1 p.u.) and 22 scenarios at a fully loaded condition (0.9 p.u.).
- Fault impedance: The vast majority (102) of scenarios simulated bolted faults, whereas four scenarios simulated high-impedance close-in faults to check the relay sensitivity.

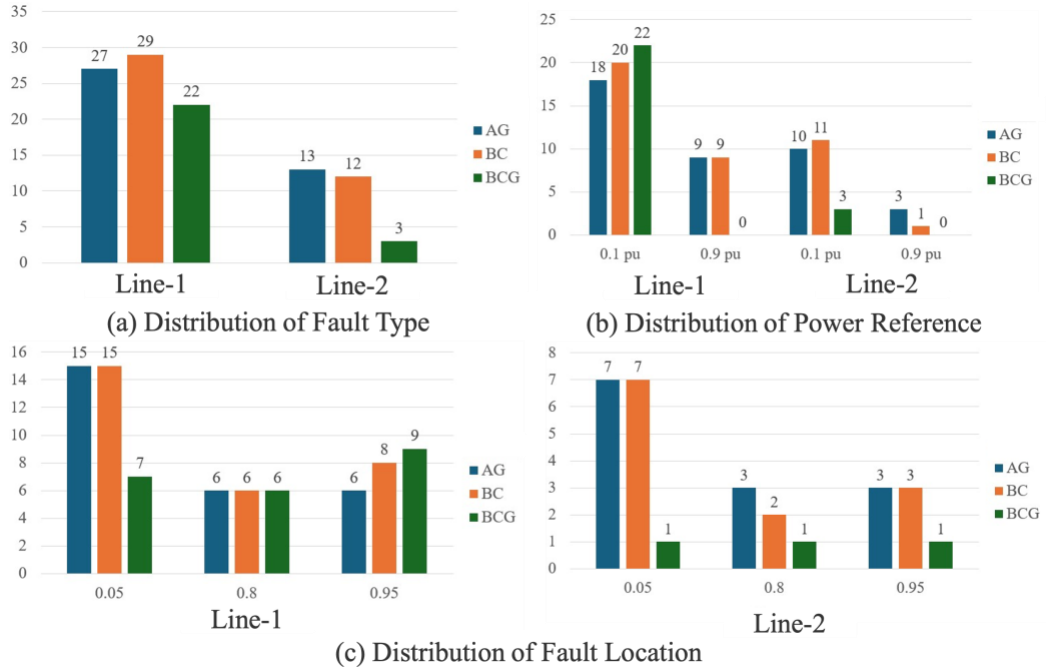


**Figure 17. Distribution of test scenarios**

Most tests were concentrated on L1, encompassing 78 scenarios, while the remaining 28 scenarios were applied to L2. The focus on L1 was due to its similarity in characteristics with L2, with the primary distinction being that L1 is longer, 113.36 miles, whereas L2 is 60.31 miles.

## 3.3 Laboratory Controller-Hardware-in-the-Loop Setup

To play the simulated fault data from the reduced PSCAD model through CHIL, instantaneous voltage and current waveforms were recorded from the current transformers and potential transformers within the PSCAD model and stored in COMTRADE format for each relay. These COMTRADE files were used as input signals to the relays through the RTDS platform. The RTDS was interfaced with the SEL-411L relays via GTAO cards, enabling real-time playback of the simulated signals. Line protection relays are connected through fiber-optic cable for differential protection to emulate field deployment. This ensured that the laboratory CHIL environment mirrored the actual field implementation, providing a robust platform for validating the relay performance under realistic operating conditions. Figure 18 shows the laboratory CHIL setup for the hardware relay testing, and Figure 19 shows the validation process of the CHIL setup. In Figure 18, the two relays on the left are used for L1 protection, and the two on the right are for L2 protection. The relays' .rdb setting files are provided by the utility partner, and three field event data are used to validate the relay settings and the current transformer and potential transformer ratios to replicate the field relay response from the event report.

The relay response comparison between the field relay and the laboratory CHIL relay is presented in Figure 20, and the time comparison is summarized in Table 13. Overall, the table shows that the laboratory CHIL relay responds faster than the field relay because of the ideal communication setup between relays. As shown in the results in Figure 20, the relay elements include 87OP, Z1P, and Z2P. For R1, all three events show some discrepancies in the communication-based differential element (87OP), with the largest discrepancy of 6.8 ms and the

smallest discrepancy of 8.3 µs. For the zone element, some discrepancies are also observed, with the largest discrepancy of 6.3 ms and the smallest discrepancy of 0.6 ms. For R4, the discrepancies are relatively smaller compared to the discrepancies observed in R1. Because the discrepancies are caused by the ideal lab setup and they are smaller than half a cycle, the results are acceptable. The fault location estimates from the CHIL simulation closely matched the actual field reports, with the calculated fault location difference remaining below 2% for all the events. The CHIL configuration effectively replicated the field behavior with similar responses.

**Figure 18. CHIL setup of SEL relays. Photos by National Laboratory of the Rockies**

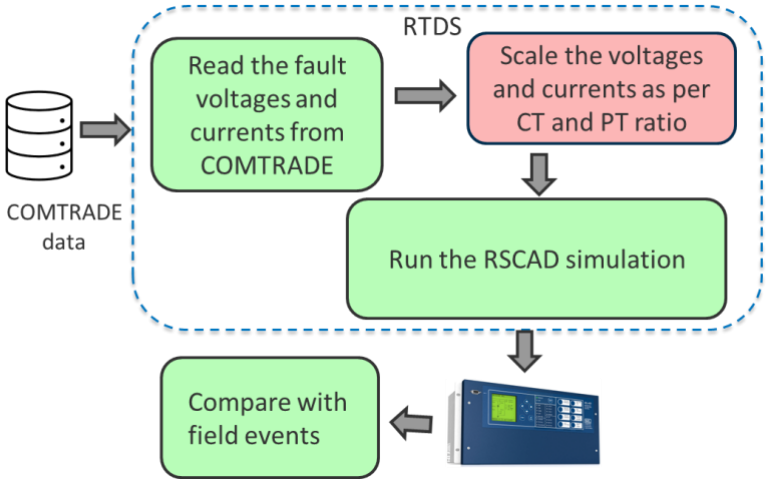


**Figure 19. Validation process of the CHIL setup**

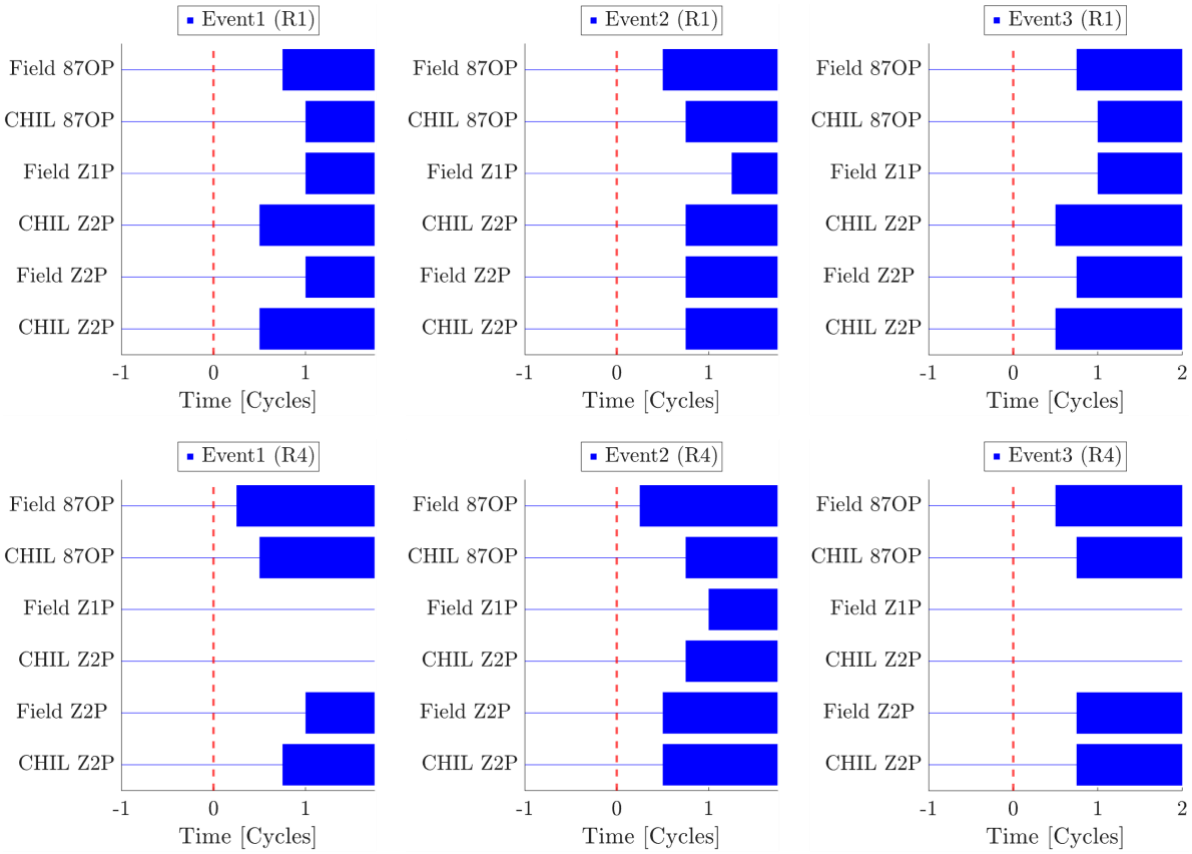


**Figure 20. Validation of the CHIL setup using field event data**

**Table 13. Validation of the CHIL Setup Using Field Event Data**

| Fault Type | Relay | 87OP Time Diff. | Zone Element Time Diff. | Fault Location | |
|---|---|---|---|---|---|
| | | | | CHIL | Field |
| Event 1 | R1 | 6.1 ms faster | 5.3 ms slower | 23.04 mi | 23.5 mi |
| | R4 | No diff. | 2.1 ms faster | 136.32 mi | 140.73 mi |
| Event 2 | R1 | 4.7 ms faster | 0.6 ms faster | 79.42 mi | 83.38 mi |
| | R4 | 6.8 ms faster | 0.6 ms faster | 80.29 mi | 81.25 mi |
| Event 3 | R1 | 8.3 µs faster | 6.3 ms slower | 33.81 mi | 32.65 mi |
| | R4 | 6.5 ms faster | 2.3 ms faster | 129.02 mi | 131.43 mi |

# 4 Results and Discussion of the Protection Study

## 4.1 Fault Study Analysis and Identification of the Protection Challenges

### *4.1.1 Initial Fault Study and Analysis Based on Normal Conditions*

Initially, we applied faults on L1 and performed a fault analysis under normal conditions, where all synchronous generators and IBRs were active. Those are the scenarios defined in Table 11, marked in gray. Two bolted faults, AG and BC, were simulated on L1, positioned at a 5% distance from bus 10 (R1), as shown in Figure 21, which is the simplified diagram of the system under study (Figure 1). The relays under test were R1 and R2 on the faulted line and R3 and R4 on the adjacent line. The results of these two tests, summarized in Table 14, show a close match between the relays' expected behavior and their actual operation.

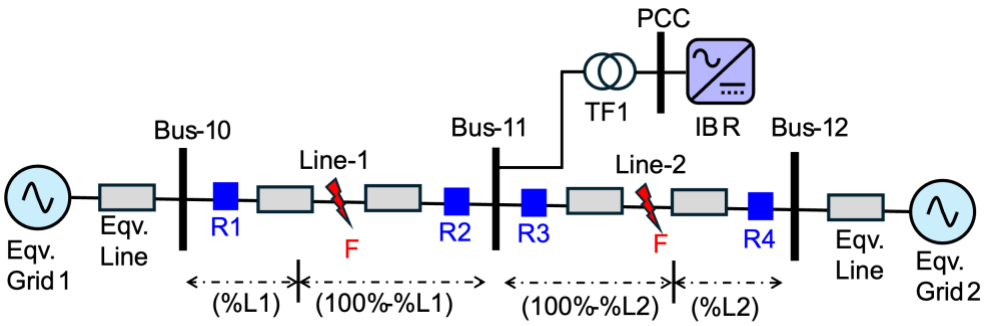


**Figure 21. Simplified circuit diagram of the system under study**

**Table 14. Summary of Relay Response During AG and BC Faults Under Normal Conditions**

| Fault Type | Relay | Element | Expected Operation | Actual Operation | Operating Time (Cycles) |
|---|---|---|---|---|---|
| AG | R1 | 87OP | Operate | Operate | 0.25 |
| | | Z1G | Operate | Operate | 0.5 |
| | | Z2G | Operate | Operate | 0.5 |
| | R2 | 87OP | Operate | Operate | 0.5 |
| | | Z2G | Operate | Operate | 1 |
| | R3/R4 | All | No op | No op | - |
| BC | R1 | 87OP | Operate | Operate | 0.75 |
| | | Z1P | Operate | Operate | 0.5 |
| | | Z2P | Operate | Operate | 0.5 |
| | R2 | 87OP | Operate | Operate | 0.75 |
| | | Z2P | Operate | Operate | 1.5 |
| | R3/R4 | All | No op | No op | - |

The analysis of the initial results confirmed that the protection system functioned reliably as intended under normal conditions, specifically with active synchronous generators on both sides of the line. The relays on L1 (R1 and R2) accurately identified and cleared the fault. Zone selectivity was validated: R1 correctly detected the fault within its primary protection zone (zone 1) and operated within 0.5 cycle. R2 demonstrated appropriate time-distance coordination, identifying the fault in its zone 2 and operating with the designated time delay of 1.0–1.5 cycles. The line differential element also operated swiftly and accurately for both relays. Notably, the relays on adjacent L2 (R3 and R4) exhibited correct selectivity by remaining stable and not operating. These successful test results under normal conditions confirm that the relay settings are accurate and reliable for systems dominated by synchronous generation. Extensive test cases give confidence to evaluate the relay performance for all scenarios, especially the IBR-only situation with weak grid scenarios.

### 4.1.2 Fault Study and Analysis for All the Scenarios

In this subsection, we present all the fault studies and the analysis for the scenarios presented in Table 11 and Table 12. We start with fault scenarios on L1, and then we test a few representative scenarios for L2 considering similar protection challenges as for L1.

#### 4.1.2.1 Phase-to-Ground Fault Analysis for Line 1

Following the initial test cases, the study proceeded with an extensive analysis of SLG (AG) faults. These tests were designed to evaluate the relay performance under progressively weaker grid conditions, including normal (gray), N-1 (blue), and IBR-only (red) contingencies, as outlined in Table 11.

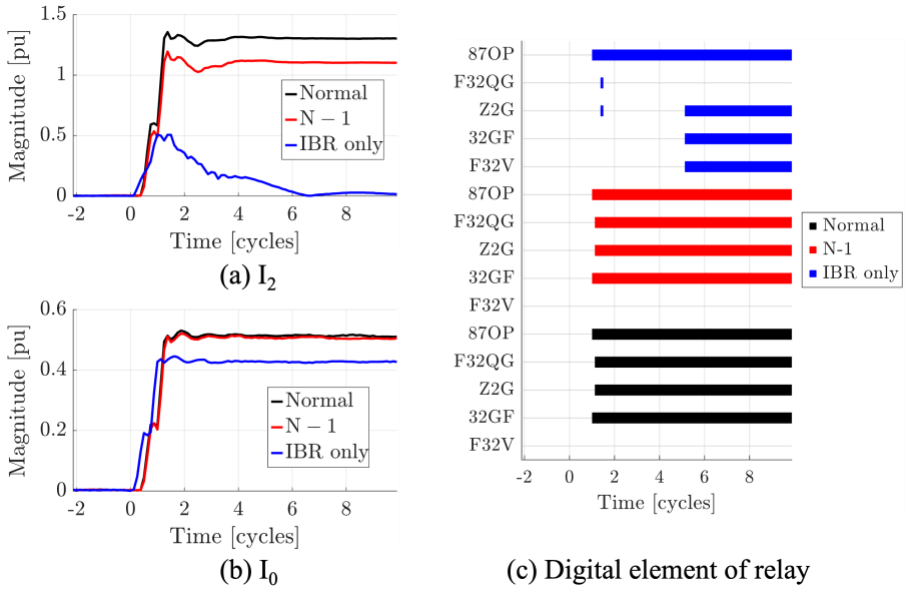


**Figure 22. Comparison of sequence components and relay responses during an AG fault under normal, N-1, and IBR-only contingencies with a 5% distance from bus 10**

All tests presented in this set were for a bolted AG fault at 5% of L1 (distance from bus 10). In the test scenarios where the synchronous generator was present (normal and N-1 contingencies), the protection relay, R1 and R2, operated correctly and rapidly, therefore indicating the reliable operation of the protection system. For the IBR-only scenario, all the protection elements in R1

operated reliably. For instance, the zone 1 (Z1G) and zone 2 (Z2G) distance elements and the differential element (87OP) all performed as expected, with operation times within 0.5 cycles, as shown in Figure 22. But R2 for the IBR-only source showed issues with the distance elements even though the differential element operated reliably and rapidly (Figure 22 (c)). In this scenario, the R2 relay's zone 2 ground distance element (Z2G) was significantly delayed, operating in 4.875 cycles, as shown in Table 15. This critical delay, which is outside the expected sub-cycle operation, revealed that the dependability of the distance protection elements is compromised under IBR-only conditions. This delay in Z2G is a direct consequence of the GFL IBR fault response, as discussed in Section 2.2.1. The IBR does not provide regulated $I_2$ during unbalanced faults, which is the fundamental problem. Note that the magnitude of the negative-sequence current momentarily increases and quickly reduces to zero, as shown in Figure 22 (a), compared to the normal and N-1 contingency. That is why the directional element F32QG quickly asserts and then de-asserts, as shown in Figure 22 (c). Under normal and N-1 conditions, the relays on the adjacent line, L2 (R3 and R4), demonstrated correct selectivity by not operating.

**Table 15. Summary of R2 Responses During an AG Fault Under Normal, N-1, and IBR-Only Contingencies**

| Contingency | R1 (Response time [cycle]) | | R2 (Response time [cycle]) | |
|---|---|---|---|---|
| | **87OP** | **Z1G** | **87OP** | **Z2G** |
| Normal (all in service) | 0.25 | 0.5 | 0.5 | 1.0 |
| N-1 contingency (IBR + N-n SGs) | 0.5 | 0.5 | 0.5 | 0.5 |
| IBR only (L2 disconnected) | 0.5 | 0.5 | 1.0 | **4.875** |

The utility partner employs a "QV" directional decision logic that prioritizes the negative-sequence directional element (32QG) over the zero-sequence element (32V). The logic for the 32Q element (F32QG) to assert during phase-to-ground faults is shown in Figure 31. It requires $I_2$ to be above its pickup setting ($a2 * I_1$ and $k2 * I_0$) and $Z2$ to be below its forward threshold ($Z2FTH$) to indicate a forward fault. In the IBR-only scenario, this logic fails [5]. The $I_2$ is sufficiently high to pass its pickup thresholds for few cycles after the fault, as shown in Figure 23 (a) and (c), making the two negative-sequence current comparators "active"; however, the phase angle between $I_2$ and $V_2$ is highly oscillatory (Figure 23 (d)). This causes the $Z2$ calculation to oscillate (Figure 23 (b)). Without a negative-sequence current leading a negative-sequence voltage 90°~100°, $Z2$ remains above the $Z2FTH$ threshold and cannot indicate the forward fault [5]. Note that $Z2$ can be calculated as in (7):

$$Z2 = \frac{Re\left[V_2\left(I_2 \times 1\angle Z_{1,\mathrm{ANG}}\right)^*\right]}{|I_2|^2} \quad (7)$$

where $Z_{1,\,ANG}$ is the positive-sequence line impedance angle. Therefore, the "QV" logic sees that the 32Q path is active ($I_2$ is high), waits for $Z2$ to go below $Z2FTH$, and blocks the 32V element. This also causes the delay in asserting the Z2G element. $I_2$ takes approximately 5.0 cycles to drop below ($a2 * I_1\ and/or\ k2 * I_0$). Only then does the 32Q logic deactivate, allowing the "best choice ground directional element" to switch to the 32V element, which then activates the F32V element (zero-sequence thresholds are met) and allows the Z2G element to operate, as shown in Figure 22. Across all tested AG fault scenarios (at 5%, 80%, and 95% of the fault locations on L1) under the IBR-only scenario, the negative-sequence directional elements (F32QG) "failed" to assert, as summarized in Table 16.

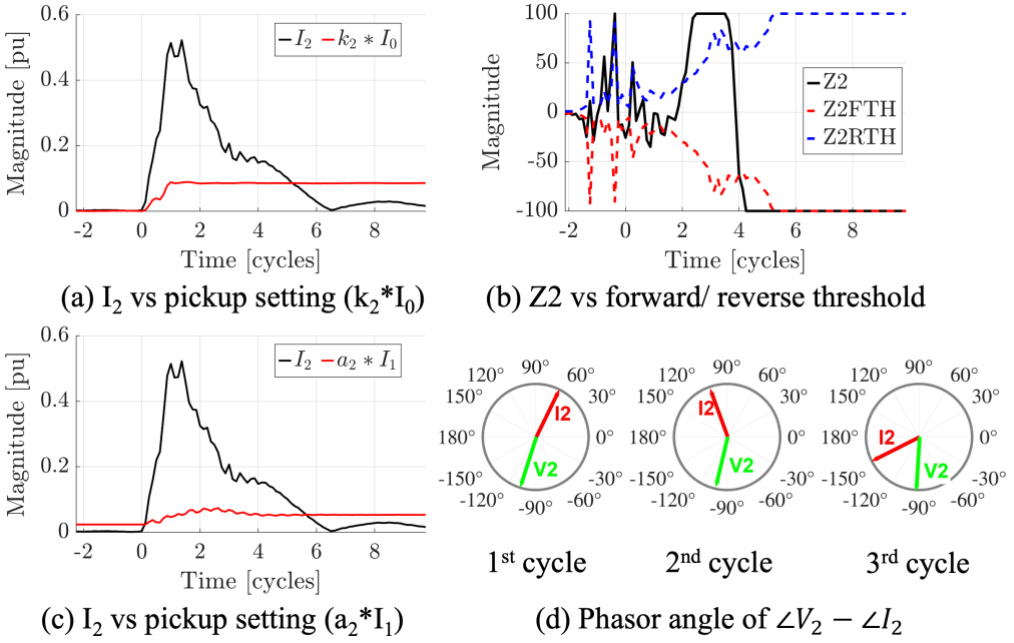


**Figure 23. Negative-sequence quantities during an AG fault in the IBR-only scenario**

Figure 24 shows the assertion times for Z1G/Z2G and F32V at 0.1-p.u. power reference. Table 15 shows the summary of the R2 response between three different fault locations and the IBR power reference with the relay response times varied from 1.5 cycles to 4.875 cycles, depending on the fault location and the IBR power reference. When the fault location is closer to the relay, the response time is 1.5 cycles. This confirms that the Z1G/Z2G elements were dependent on the 32V logic, which only became active after the relay's internal logic shifted from 32Q to 32V.

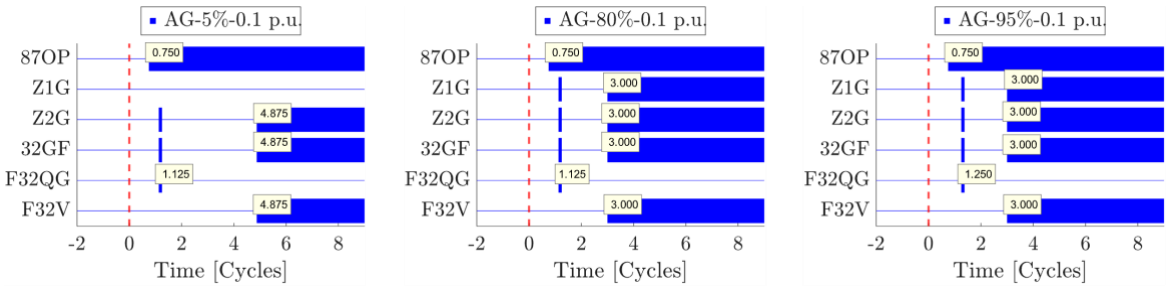


**Figure 24. R2 responses during AG faults under the IBR-only scenarios**

**Table 16. Summary of the R2 Responses During AG Faults Under the GFL IBR-Only Scenarios**

| Element | 5% 0.1 p.u. | 5% 0.9 p.u. | 80% 0.1 p.u. | 80% 0.9 p.u. | 95% 0.1 p.u. | 95% 0.9 p.u. |
|---|---|---|---|---|---|---|
| Z1G/Z2G assertion time (cycle) | Z2G: 4.875 | Z2G: 3.375 | 3.0 | 2.375 | 3.0 | 1.5 |
| F32V assertion time (cycle) | 4.875 | 3.375 | 3.0 | 2.375 | 3.0 | 1.5 |
| F32QG assertion time (cycle) | Failed | Failed | Failed | Failed | Failed | Failed |

#### *4.1.2.2 Phase-to-Phase and Phase-to-Phase-to-Ground Fault Analysis*

The simplified schematic diagram of the relay phase distance logic is shown in Figure 25. For the zone 2 phase distance element (Z2P) to operate, three conditions must be met simultaneously: (1) A negative-sequence directional element (F32Q/F32P) must be asserted, (2) the phase fault current (IBC) must exceed the overcurrent pickup (Z50P), and (3) the measured mho distance quantity (MBC) must be inside the mho circle reach Z2MP. Similarly, zone 1 follows the same logic, with zone 1 reaching the setting Z1MP.

Figure 26 shows that under normal and N-1 contingencies, a high fault current and the 32Q element from synchronous generators correctly and reliably assert relay elements (87OP, Z2P and F32P) for a fault with 5% distance from bus 10. In contrast, the distance (Z1P/Z2P) and directional (F32P/F32Q) protection elements during a phase-to-phase (BC) and phase-to- phase-to-ground (BCG) faults completely failed to operate under all IBR-only scenarios, unlike the AG faults, which were merely delayed due to the absence of a negative sequence. For the IBR-only scenarios (including normal and N-1), the mho distance element met condition 3 (Figure 26 (b) shows $M_{BC}$ drops below Z2MP.Set). The fault current (IBC) was insufficient to activate the overcurrent supervision element (Figure 26 (a) shows the fault current is less than the threshold), and therefore condition 2 is not met.

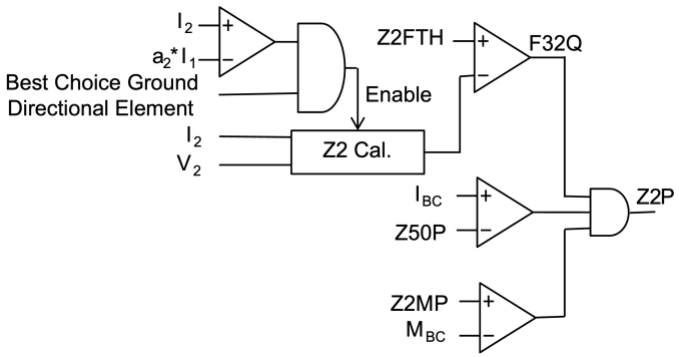


**Figure 25. Schematic diagram of the phase distance element (Z2P) [5]**

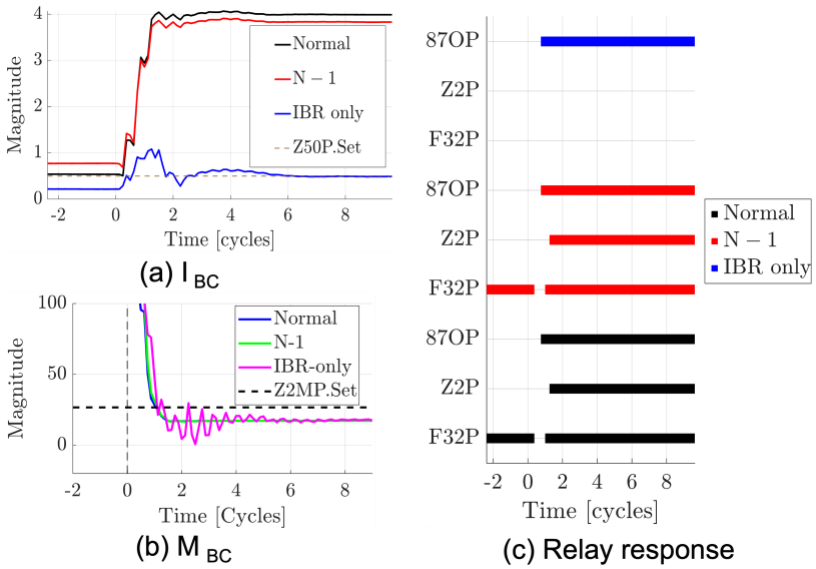


**Figure 26. Comparison of phase-to-phase quantities and relay responses during a BC fault under normal, N-1, and IBR-only contingencies for a fault with 5% distance from bus 10**

Simultaneously, condition 1 (directional F32Q element) fails because the nonregulated $I_2$ of the IBR creates an unstable $\angle I_2 - \angle V_2$ angle, as discussed in Section 4.1.2.1. The testing results are shown in Figure 27 and Figure 28. This instability causes the measured Z2 to remain above its forward threshold ($Z2FTH$), causing the directional element (F32Q) to fail, as noted in Table 17. Note that F32P also relies on F32Q, which causes F32P to fail as well. Because both the directional and overcurrent supervision logics failed, the Z2P element was blocked and could not operate even though the fault was within its impedance reach. For BCG faults, the relay applies the same logic for BC faults. This design choice is intentional: The relay prefers to use negative-sequence ($I_2$) quantities for directionality over zero-sequence ($I_0$) quantities. This is because $I_2$ is generally considered more reliable, especially in systems with a high zero-sequence impedance, where $I_0$-based directional elements can become unreliable. This reliance on $I_2$ is precisely what causes the failure in the IBR-only scenarios. Across all the tested IBR-only BC and BCG fault scenarios (at 5%, 80%, and 95% of the fault locations on L1), the negative-sequence directional elements (F32Q) "failed" to assert, and the phase-to-phase overcurrent supervision element stayed de-asserted due to a low fault current. blocks Z1P/Z2P distance elements from operating for both BC and BCG faults summarized in Table 17. This left the differential 87OP element as the only line of defense.

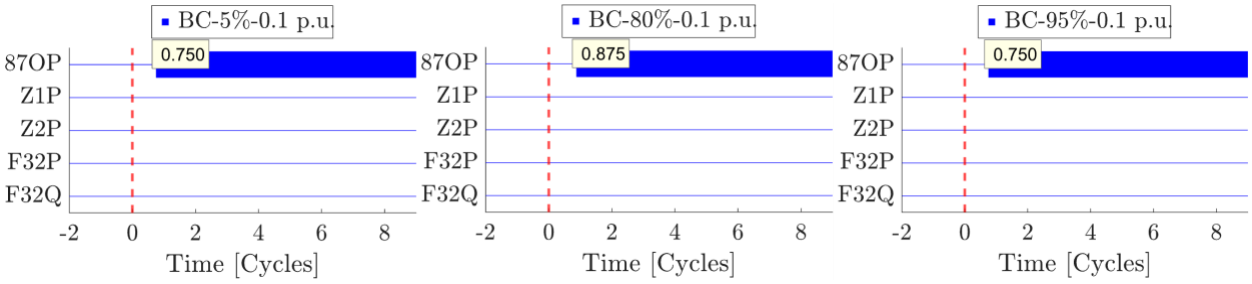


**Figure 27. Relay responses under the IBR-only scenarios during BC faults**

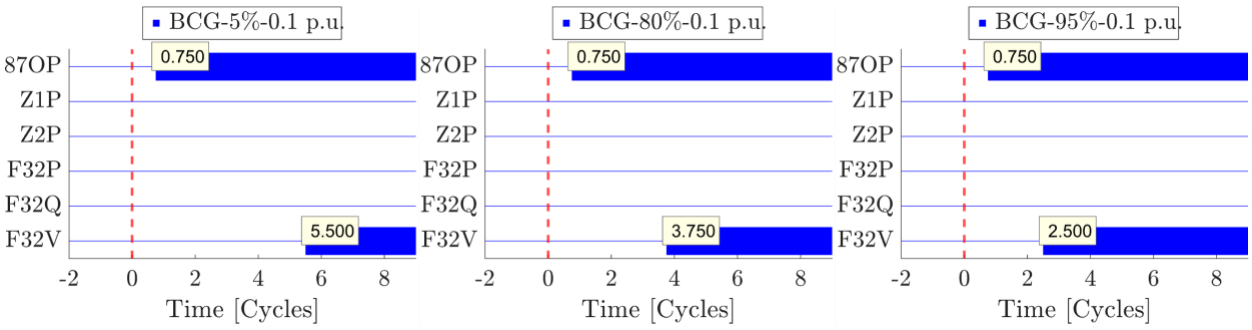


**Figure 28. Relay responses under the IBR-only scenarios during BCG faults**

**Table 17. Summary of R2's Performance Under IBR-Only Scenarios During BC and BCG Faults**

| Element | BC Fault 5% 0.1 p.u. | BC Fault 80% 0.1 p.u. | BC Fault 95% 0.1 p.u. | BCG Fault 5% 0.1 p.u. | BCG Fault 80% 0.1 p.u. | BCG Fault 95% 0.1 p.u. |
|---|---|---|---|---|---|---|
| Z1P/Z2P assertion time (cycle) | Failed | Failed | Failed | Failed | Failed | Failed |
| F32Q/F32P assertion time (cycle) | Failed, Z2 above Z2FTH | Failed, Z2 above Z2FTH | Failed, Z2 above Z2FTH | Failed, Z2 above Z2FTH | Failed, Z2 above Z2FTH | Failed, Z2 above Z2FTH |

### *4.1.3 Fault Analysis for Line 2*

A set of fault scenarios, as detailed in Table 12, was assessed on L2. L2 is considerably shorter (63 miles) than L1 (113 miles), resulting in reduced positive- and zero-sequence impedance magnitudes. Despite these physical differences, R3 demonstrated performance issues similar to those observed for R2 during faults at L1 under IBR-only scenarios. Figure 29 shows the response of R3 for AG, BC, and BCG faults at 5%, 80%, and 95% of the locations with a 0.1-p.u. IBR power reference.

Similar to the results for L1, the negative-sequence directional element (32Q) failed to assert the AG fault decisions due to the unregulated negative-sequence current. Consequently, the relay had to rely on the zero-sequence directional element (F32V) after a time delay. As shown in Figure 29 (top row), although the relay successfully cleared the faults, its operation was consistently delayed. The Z2G/Z1G asserted at 3.25, 2.625, and 2.5 cycles for 5%, 80%, and 95% of the L2 fault locations, respectively, which aligned with the F32V assertion. This confirms that the directional logic delays due to shifting from "Q" to "V" are a systemic issue in the IBR-only scenarios during AG faults regardless of the line length.

The performance for phase-to-phase faults was unreliable. As shown in Figure 29 (middle row), the relay local elements (Z1P/Z2P, F32P, and F32Q) completely failed to operate during the BC fault at 80% and 95% of the L2 locations and operated at 3.375 cycles at 5% of the L2 locations. Similarly, R3 cannot operate based on the phase distance element during phase-to-phase-to-ground faults, as shown in Figure 29 (bottom row), for all three fault locations. Without regulating the negative-sequence current, the existing phase distance protection scheme becomes unreliable.

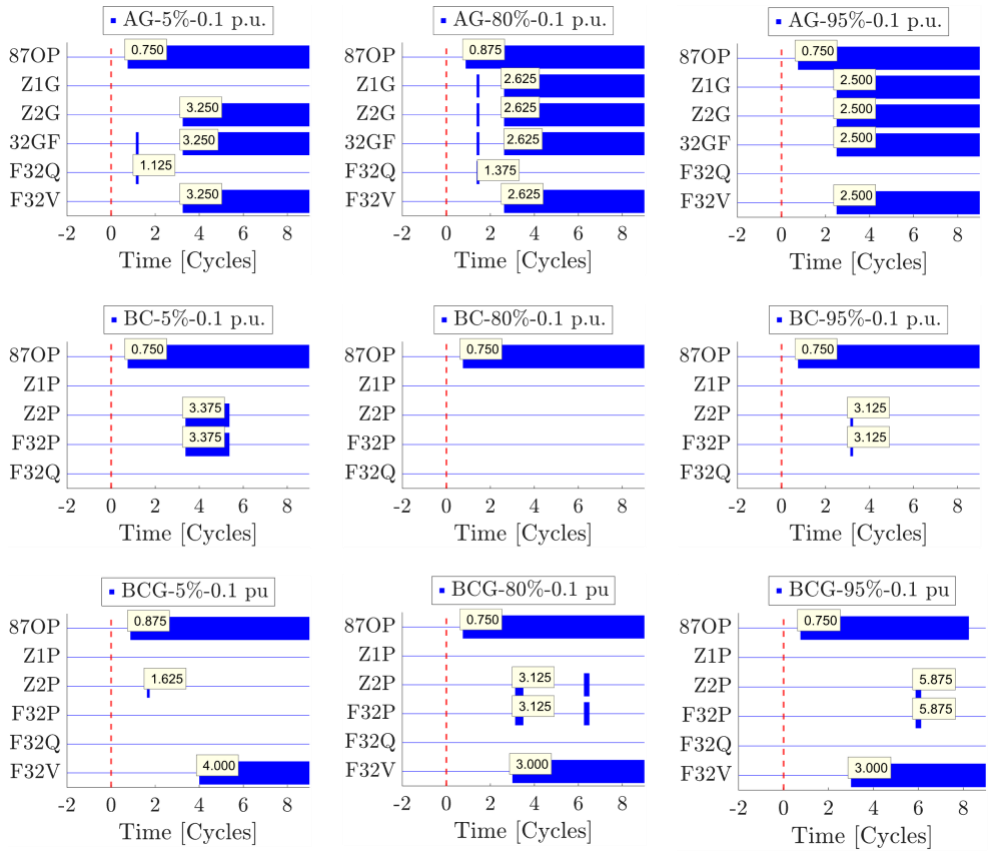


**Figure 29. R3 responses during AG, BC, and BCG faults at L2 under the IBR-only scenarios**

## 4.2 Proposed Enhanced Protection Strategies

Based on the results of the fault study and analysis, the existing protection schemes either failed or experienced significant delays under the IBR-only contingencies, so certain improvements were suggested. The main objective is to guarantee dependable and reliable operation (ranging from the sub-cycle to three cycles) for both phase-to-ground and phase-to-phase faults while maintaining security during regular grid operations.

### *4.2.1 Strategy for Phase-to-Ground Fault: Prioritizing Zero-Sequence Directionality*

The delayed tripping during AG faults under the IBR-only scenarios was traced to the relay's default "best choice ground directional element" logic. With the default ORDER = QV setting, the relay prioritizes the negative-sequence element (32Q) . As detailed in Section 4.1.2.1, the unregulated $I_2$ from the IBR causes the 32Q logic to remain in an intermediate state, preventing the zero-sequence element (32V) from engaging until the $I_2$ magnitude diminishes. We propose two strategies for addressing phase-to-ground faults. Option 1 suggests altering the order of the directional element priority setting from QV to V. (See the following section, 4.2.2, for Option 2.) By configuring ORDER = V, the relay is compelled to disregard the negative-sequence directional element (32Q) and rely solely on the zero-sequence directional element (32V) to determine the ground fault directionality. This change in directional element priority ORDER from QV to V makes the relay rely on the zero-sequence parameters, zero-sequence current restraint factor ($a_0$), and zero-sequence forward threshold ($Z0FTH$) [6].

Zero-sequence quantities ( $V_0$ and $I_0$) are mainly influenced by passive system grounding, such as the grounding topology shown in Figure 8, unlike unregulated negative-sequence quantities of the IBRs during unbalanced faults, as shown in Figure 23. In the IBR-only scenario, the zero-sequence current ($I_0$) and voltage ($V_0$) remained stable and effective for the fault detection, as shown in Figure 22 (b). By prioritizing V, the relay uses the zero-sequence ground directional element logic (Figure 30), Figure 30where the $Z0FTH$ threshold establishes the boundary for the forward direction. Because the system grounding remains unchanged regardless of the IBR control mode, this threshold remains reliable. When the magnitude of the zero-sequence current ($I_G$ or $3I_0$) exceeds the positive-sequence current scaled by the restraint factor, $a_0$ (i.e., $|I_0| > a_0 \cdot |I_1|$), the relay calculates the zero-sequence impedance quantities ($Z0$) using Eq. 8:

$$Z0 = \frac{Re\left[3V_0\left(I_G \times 1\angle Z_{0,\mathrm{ANG}}\right)^*\right]}{|I_G|^2} \tag{8}$$

where $Z_{0,\ \mathrm{ANG}}$ is the zero-sequence line impedance angle.

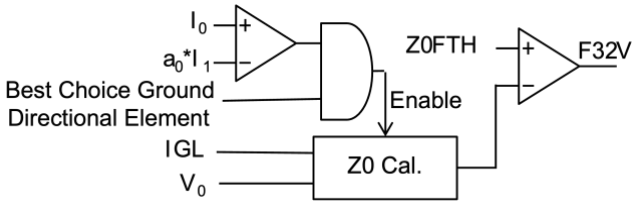


**Figure 30. Schematic diagram of the zero-sequence directional element for a phase-to-ground fault (F32V) [5]**

If the calculated $Z0$ is less than the $Z0FTH$, the element identifies a forward fault. The $a_0$ prevents incorrect operation during unbalanced conditions or current transformer saturation, ensuring that the element only functions when the ratio $|I_0|/|I_1|$ is substantial. It eliminates the delay caused by the failed 32Q element, as discussed in Section 4.1.2.1. The relay immediately processes stable zero-sequence quantities and asserts the F32V element when the respective quantities exceed the threshold.

### *4.2.2 Strategy for Phase-to-Ground Fault: Tuning of Restraining Factors*

Option 2 seeks to maintain the preferred ORDER = QV directional logic, capitalizing on the enhanced sensitivity of the 32Q under robust grid conditions while addressing the delay experienced in the IBR-only scenarios by adjusting the pickup threshold. Central to this strategy is the increase in the positive-sequence current restraint factor, $a_2$, and the zero-sequence current restraint factor, $k_2$ [6]. These factors are crucial settings within the relay logic for determining when negative-sequence quantities are present and adequate, as shown in Figure 31. The factor $a_2$ is the ratio of the negative-sequence current to the positive-sequence current ($I_1$), $|I_2|/|I_1|$, whereas $k_2$ is the ratio of the negative-sequence current to the zero-sequence current ($I_0$), $|I_2|/|I_0|$. 32Q remains active and asserts its priority only as long as the measured $I_2$ exceeds the threshold set by these two restraining factors. By increasing $a_2$ and $k_2$, the pickup thresholds ($|a_2 \cdot I_1\ |$ and $|k_2 \cdot I_0|$) are raised to disable the Z2 calculation and block the F32QG element, as shown in Figure 31.

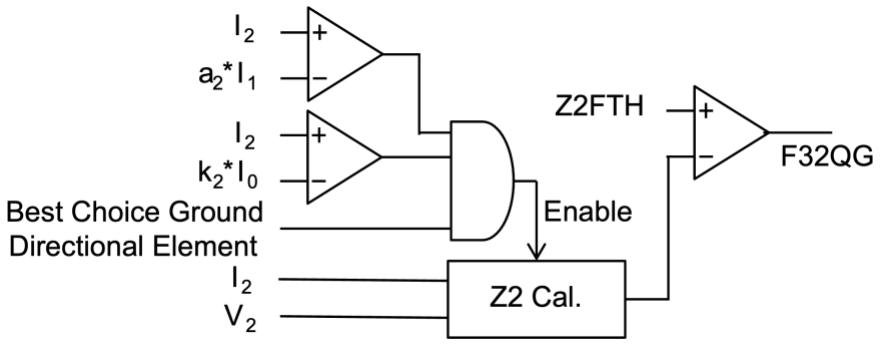


**Figure 31. Schematic diagram of the negative-sequence directional element for a phase-to-ground fault (F32QG) [5]**

During IBR-only contingencies, the unregulated $I_2$ is already very low and oscillatory, as shown in Figure 23. With higher pickup thresholds, the IBR's low $I_2$ magnitude will fall below the required threshold much faster than with the default settings. When $|I_2|$ drops below the elevated $|a_2 \cdot I_1|$ or $|k_2 \cdot I_0|$ thresholds, the relay internal logic determines that the negative-sequence quantities are no longer sufficient or reliable, causing the 32Q logic path to be deactivated sooner. This accelerated deactivation allows the "QV" logic to immediately switch the priority to the 32V element. The 32V element, which relies on stable $V_0$ and $I_0$ quantities from the transformer grounding, asserts quickly, eliminating the critical three- to four-cycle waiting period and reducing the overall trip time of the Z1G/Z2G distance elements. This strategy maintains security during normal and N-1 contingencies because the synchronous generators still contribute a significant amount of reliable negative-sequence current. This higher $I_2$ magnitude remains well above the increased $|a_2 \cdot I_1|$ and $|k_2 \cdot I_0|$ thresholds, ensuring that the 32Q element retains its priority and performs reliably in all grid scenarios.

### 4.2.3 Strategy for Phase-to-Phase and Phase-to-Phase-to-Ground Faults

The complete inadequacy of traditional phase distance protection in addressing phase-to-phase and phase-to-phase-to-ground faults necessitates a strategic reorientation of the core direction and supervision logic. This proposed strategy intentionally discards the use of unreliable negative-sequence components, replacing them with novel directional and supervisory elements based on stable positive-sequence quantities. This approach is formalized in the custom relay logic diagram shown in Figure 32Figure 32Figure 32.

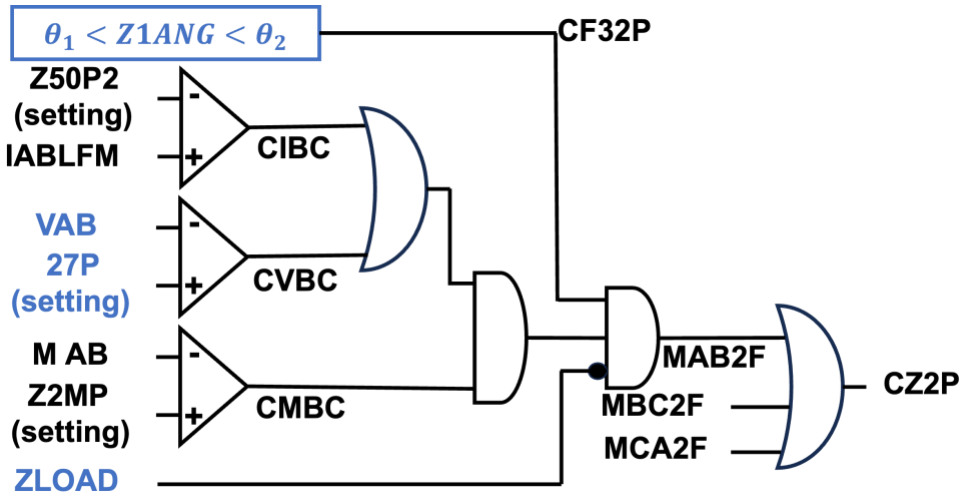


**Figure 32. Schematic diagram of the zone 2 enhanced phase distance element**

#### *4.2.3.1 Directional Logic: Positive-Sequence Directional Element (C32P)*

The strategy replaces the failed negative-sequence directional element (F32P/F32Q) with a positive-sequence angle-based directional element (C32P). Positive-sequence quantities ($V_1$, $I_1$) are generally the most stable during a fault, as they are least affected by IBR control dynamics and unbalanced conditions, making the directional decision reliable when $I_2$ fails. The directional decision is based on the angle (Z1ANG) calculation C32P, which uses the angle between the positive-sequence voltage ($\angle V_1$) and the positive-sequence current ($\angle I_1$) to determine the direction using Eq. 9:99

$$C32P = \theta_1 < Z1ANG < \theta_2; \quad Z1ANG = [\angle V_1 - \angle I_1] \tag{99}$$

Angle $\theta_1$ and $\theta_2$ are influenced by the positive-sequence line impedance angle and network topology. For example, when an IBR is connected to the grid through a delta-wye transformer configuration, a 30° phase shift is introduced to the voltage. Consequently, the measured angle will exhibit a minimum of 30°, with an additional angle determined by the line impedance between the IBR terminal and the point of common coupling for close-in faults. This angle increases to 30° plus the positive-sequence line impedance angle for remote faults. A forward fault is identified when the calculated angle falls within the defined secure sector.

#### *4.2.3.2 Enhanced Supervision and Adaptivity*

The conventional supervision based on the phase overcurrent element ($I_{BC} > Z50P$) is unreliable because of the insufficient fault current contribution of the IBR. The enhanced strategy addresses this issue through adaptive supervision. An undervoltage element (27P) was introduced for primary supervision under IBR-only scenarios. A significant and immediate voltage sag is a highly reliable fault indicator in this weak grid area because IBRs are weak sources and can have a substantially larger voltage drop than that of traditional synchronous generators. The 27P element is enabled when the phase-to-phase voltage (VAB) drops below an adaptive threshold (27P setting). This undervoltage element is OR-gated with the overcurrent element. The system uses adaptive 27P settings that are adjusted to activate only during IBR-only contingencies, where the voltage sag is more significant. This ensures that for normal and N-1 contingencies

(where synchronous generators stabilize the fault current), the more reliable overcurrent element continues to be used for supervision.

The final assertion of the phase distance elements relies on strict adherence to security protocols, including load encroachment checks. The load encroachment logic prevents the misinterpretation of a heavy system load as an internal fault. The relay monitors the positive-sequence load impedance ($ZLOAD$) for both export and import conditions, asserting a decision when the measured impedance falls within the corresponding load region. This logic, which operates only when the ($I_1$) exceeds a minimum threshold (e.g., 10% of nominal current), blocks the positive-sequence directional element (C32P) from tripping on load.

The final output, $CZ$2P, is asserted if any phase combination is successfully asserted (MAB2F OR MBC2F OR MCA2F), providing comprehensive tripping coverage for all phase-to-phase fault types (AB, BC, CA) within zone 2. The custom logic follows an identical structure for zone 1 faults, using the zone 1 reach threshold (Z1MP) to ensure that both zones are secured by the same enhanced directional and supervisory elements.

#### 4.2.3.3 Verifying the Proposed Enhanced Protection for Phase-to-Phase and Phase-to-Phase-to-Ground Faults

The validation of the enhanced protection scheme for phase-to-phase (BC) and phase-to-phase-to-ground (BCG) faults was performed using a comprehensive set of simulation scenarios. Figure 33 shows the distribution of these validation cases, which were strategically selected to encompass a range of fault types (LL, LLG) (Figure 33 (a)), locations (5%, 50%, 80%, and 95%) (Figure 33 (b)), and IBR power references (0.1 p.u. to 0.95 p.u.) (Figure 33 (c)). This comprehensive testing ensures the efficacy of the proposed logic so that it works reliably and robustly under diverse system operating conditions.

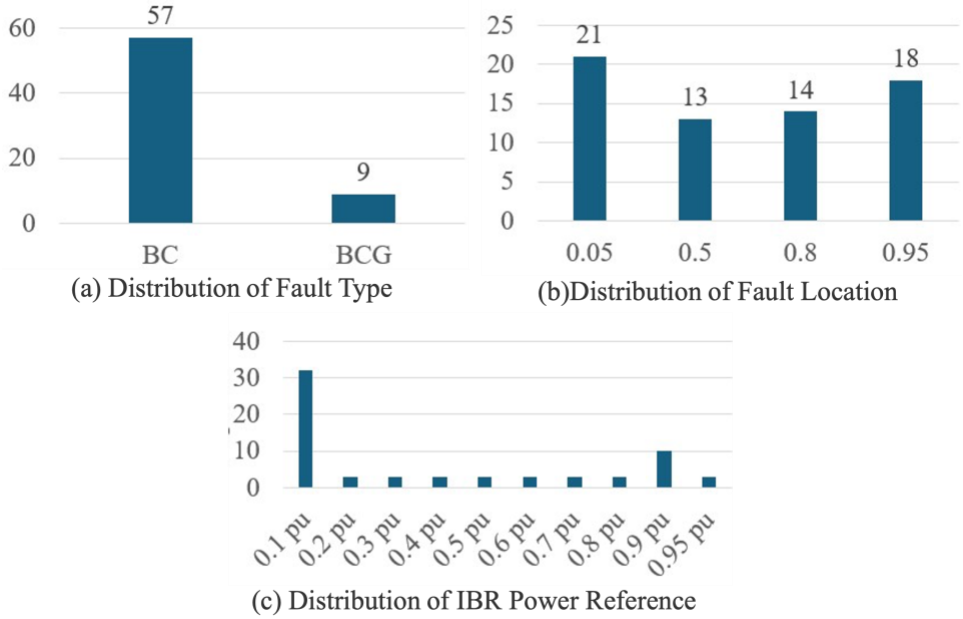


**Figure 33. Distribution of the enhanced phase-to-phase fault protection scheme's validation scenarios**

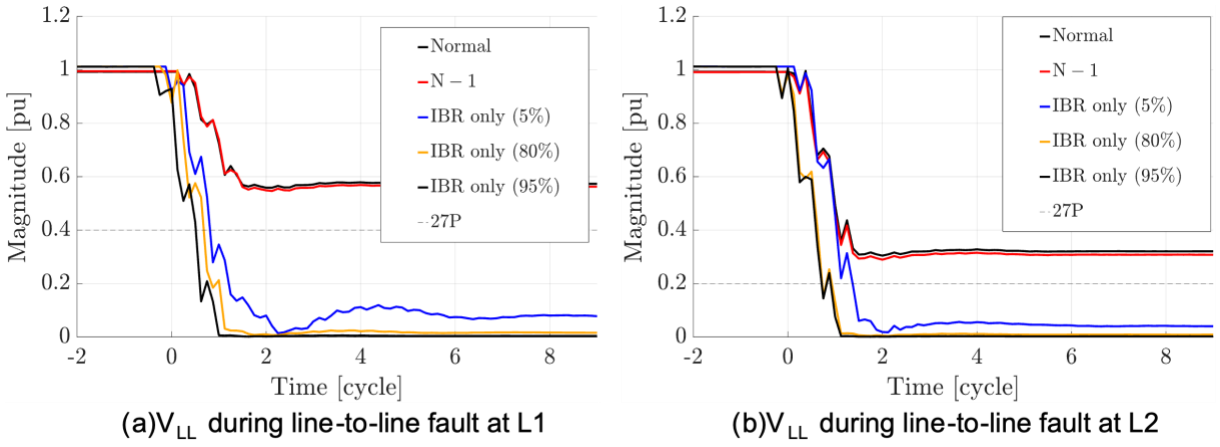


**Figure 34. Magnitude of $V_{LL}$ during phase-to-phase faults under normal, N-1, and IBR-only scenarios**

A critical component of the enhanced protection scheme for phase-to-phase and phase-to-phase-to-ground faults is the undervoltage supervision element (27P). Its efficacy is supported by the distinct voltage sag characteristics observed between synchronous generator-dominated (normal, N-1) and IBR-only scenarios. As shown in Figure 34, the magnitude of the line-to-line voltage ($V_{LL}$) significantly differs between these operating modes. For faults on L1, synchronous generator-dominated scenarios (normal and N-1) maintain a voltage sag above 0.5 p.u., whereas IBR-only scenarios result in deeper sags below 0.4 p.u (Figure 34 (a)). Similarly, for faults on L2, the synchronous generator-dominated scenarios remain above 0.3 p.u., whereas the IBR-only scenarios drop below 0.2 p.u. (Figure 34(b)). This distinct separation in voltage magnitude confirms that an adaptive undervoltage threshold can effectively distinguish fault conditions in IBR-only scenarios in which the fault current is insufficient for supervision.

The reliability of the directional decision of the enhanced protection scheme relies on the positive-sequence impedance angle (Z1ANG), the bounds of which are dictated by the network topology connecting the IBR to the grid. The point-of-common-coupling path includes a delta-wye transformer and a wye-wye-delta three-winding transformer, separated by an interconnecting line segment. This configuration introduces an inherent phase shift that comprises the transformer's 30° shift plus an additional angle ($\varepsilon$) contribution from the interconnection line. Given a positive-sequence line impedance angle of the transmission line (L1 and L2) of approximately 85°, the expected Z1ANG for a forward fault theoretically ranges from a minimum of $30° + \varepsilon$ for close-in faults to a maximum of $30° + \varepsilon + 85°$ for remote faults. These theoretical expectations were supported by the simulation results presented in Figure 35Figure 35. For forward faults on both L1 and L2, the observed angle consistently fell within the range of 55° to 125° (Figure 35Figure 35 (a) and (b)). Conversely, for reverse faults, the Z1ANG shifts distinctly to a range between $-60°$ and $-150°$ (Figure 35 Figure 35(c)). This clear angular separation validates the security of the chosen directional sector settings in the enhanced scheme.

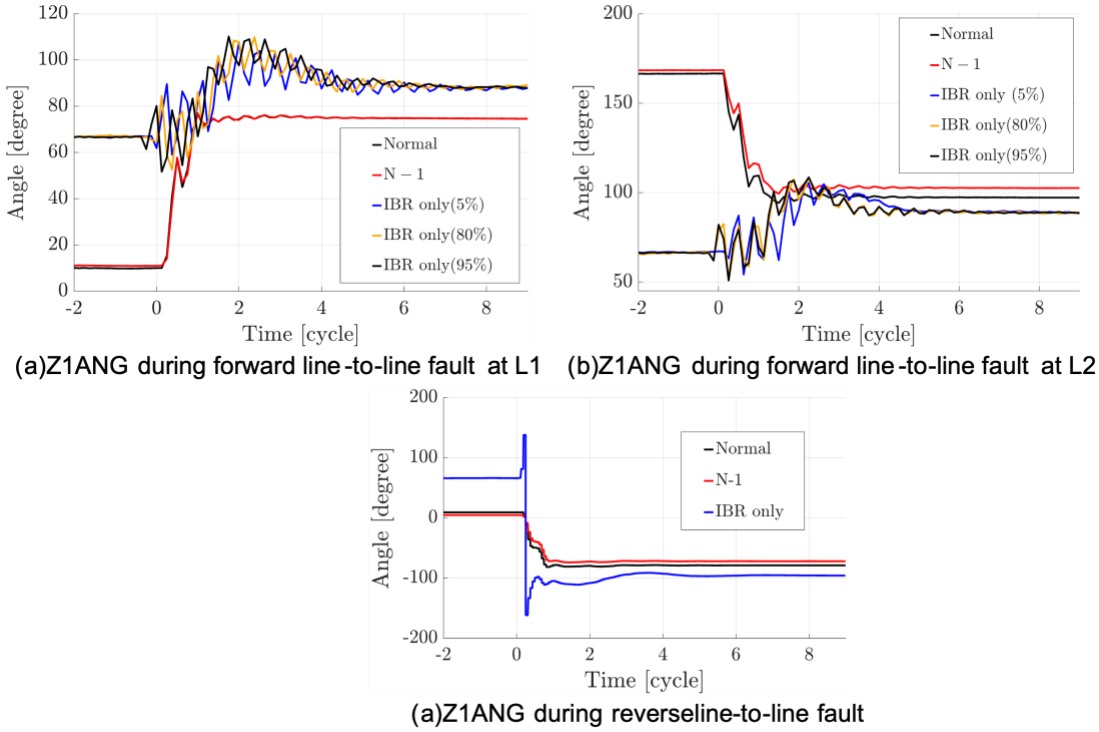


(a)Z1ANG during forward line-to-line fault at L1 (b)Z1ANG during forward line-to-line fault at L2

(a)Z1ANG during reverseline-to-line fault

**Figure 35. Magnitude of Z1ANG during a phase-to-phase fault under normal, N-1, and IBR-only scenarios**

## 4.3 Evaluation of the Enhanced Protection

This subsection validates the effectiveness of the proposed strategies for mitigating directional logic delays during phase-to-ground faults as well as enhanced protection schemes for phase-to-phase and phase-to-phase-to-ground faults. The evaluation considers dependability and reliability across normal, N-1, and IBR-only operating scenarios.

### *4.3.1 Evaluation of Proposed Strategies for Phase-To-Ground Fault*

The evaluation focused on the IBR-only scenarios (0.1-p.u. power reference), which exhibited the most significant operational delay under the default settings. Figure 36 shows the fault current comparison at different distance during AG fault. Note that the fault current magnitude significantly reduced at 5% distance. Both proposed enhancement strategies successfully speed up the Z1G/Z2G assertion time across all the tested scenarios compared to the default setting, which experienced delays up to 4.875 cycles.

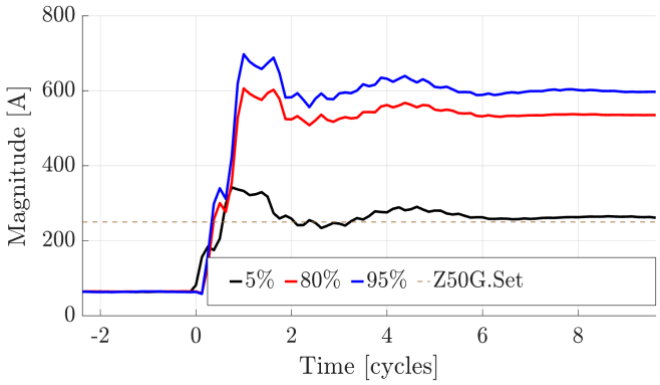


**Figure 36. Fault current comparison during an AG fault under the IBR-only scenarios**

#### 4.3.1.1 Prioritizing Zero-Sequence Directionality

By configuring the directional priority to ORDER = "V," the relay deactivated the negative-sequence directional element (32Q/F32QG) and functioned based on the zero-sequence element (F32V). This method demonstrated reliability for the zone 1 fault locations (80% and 95%), achieving trip times of less than 1.0 cycle, which represents a significant improvement over the 3.0 cycles with the default, as shown in Figure 37 (b) and (c). The relay reliably asserted the F32V element based on stable zero-sequence quantities ($V_0$, $I_0$, Z0) and enabled the distance element Z1G. At remote fault locations, such as the 5% fault location, Z2G was asserted in 1.125 cycles, followed by the assertion of F32V; however, the extended line length (113.36 miles) substantially increased the impedance, thereby reducing the fault current. Consequently, the fault current (IA) temporarily fell below the supervision threshold (Z50G) due to transients during the first three cycles after the fault at two cycles, and it remained there for approximately 1.5 cycles, as shown in Figure 36, causing the Z2G element to de-assert (Figure 37 (a)). Nevertheless, Z2G subsequently reasserted at 3.375 cycles. Overall, the use of zero-sequence elements significantly enhanced the relay response times and reliability across different fault locations.

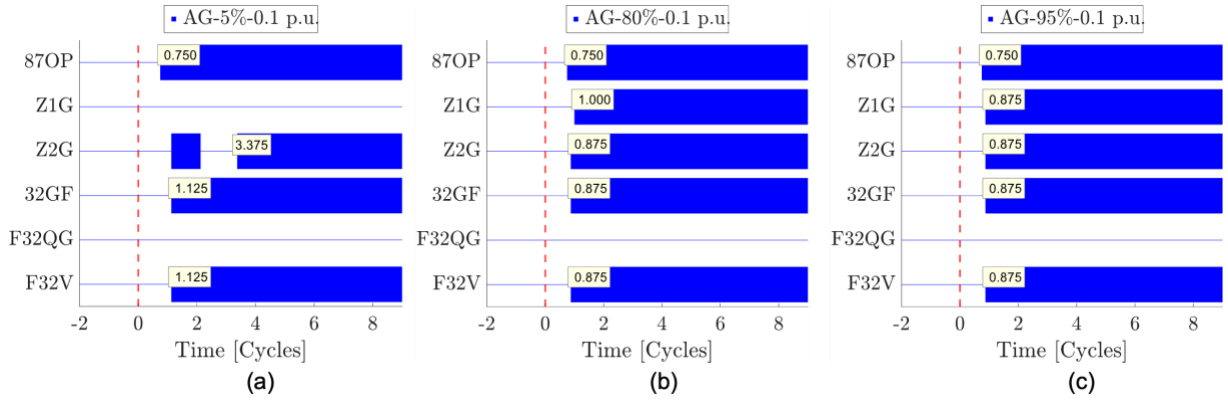


**Figure 37. Relay response during AG faults under IBR-only scenarios with ORDER = "V"**

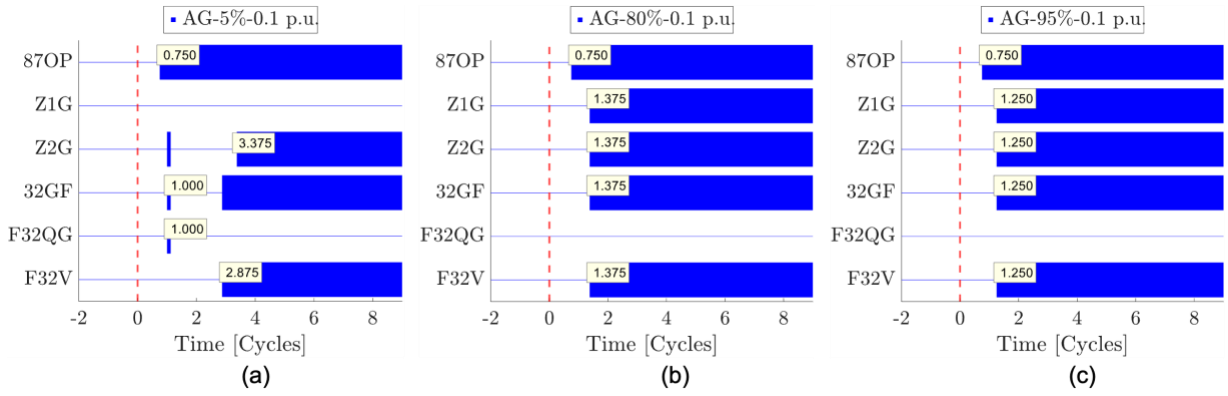


**Figure 38. Relay response during AG faults under IBR-only scenarios with tuned a2 and k2**

### 4.3.1.2 Tuning Restraining Factors

The strategy for tuning the restraining factors involved maintaining the ORDER = "QV" logic while increasing the restraining factors (a2 and k2) to elevate the current pickup thresholds. The elevated thresholds more swiftly prompted the deactivation of the 32QG logic path, thereby enabling the relay to more rapidly prioritize the F32V element. This approach effectively reduced the Z2G assertion time for the fault at 80% and 95% of the locations from 3.0 cycles to 1.375 cycles and 1.25 cycles, respectively, as shown in Figure 38. Although this option was faster than the default, it was marginally slower than the previous strategy (summarized in Table 18). The Z2G time at 80% of the fault locations was 1.375 cycles compared to 0.875 cycles for Option 1 and 1.25 cycles compared to 0.875 cycles at 95% of the fault locations. This discrepancy arises because the logic still requires a brief waiting period (the time necessary for $I_2$ to fall below the adjusted threshold) before transitioning to F32V. The speed can be further enhanced by increasing the I2 thresholds while ensuring reliable operation of the relay under normal and N-1 scenarios. As previously discussed, the remote location fault momentarily de-asserts for low fault currents (Figure 36) and ultimately asserts at 3.375 cycles (Figure 38). Both options offer a reliable solution for AG faults, clearing the zone 1 fault in less than 1.5 cycles, as summarized in Table 18.

**Table 18. Comparison of R2 Response During an AG Fault With Different Protection Strategies**

| | **Default** | | **ORDER = "V"** | | **Tuned $a_2$ and $k_2$** | |
|---|---|---|---|---|---|---|
| **Fault Characteristics (IBR-Only)** | **Z1G/Z2G Assertion Time (Cycle)** | **F32V Assertion Time (Cycle)** | **Z1G/Z2G Assertion Time (Cycle)** | **F32V Assertion Time (Cycle)** | **Z1G/Z2G Assertion Time (Cycle)** | **F32V Assertion Time (Cycle)** |
| 5%–0.1 p.u. | 4.875 | 4.875 | 3.375 | 1.125 | 3.375 | 2.875 |
| 80%–0.1 p.u. | 3.0 | 3.0 | 0.875 | 0.875 | 1.375 | 1.375 |
| 95%–0.1 p.u. | 3.0 | 3.0 | 0.875 | 0.875 | 1.25 | 1.25 |

### 4.3.2 Evaluation of Enhanced Protection for Phase-to-Phase and Phase-to-Phase-to-Ground Faults

The efficacy of the proposed enhanced protection strategy for phase-to-phase and phase-to-phase-to-ground faults was evaluated across a complete spectrum of grid operating conditions, encompassing normal operation, N-1 contingencies, and IBR-only scenarios on both L1 and L2. This extensive testing ensured that the strategic shift from negative- to positive-sequence directional logic, coupled with undervoltage supervision, provided the necessary dependability without compromising security.

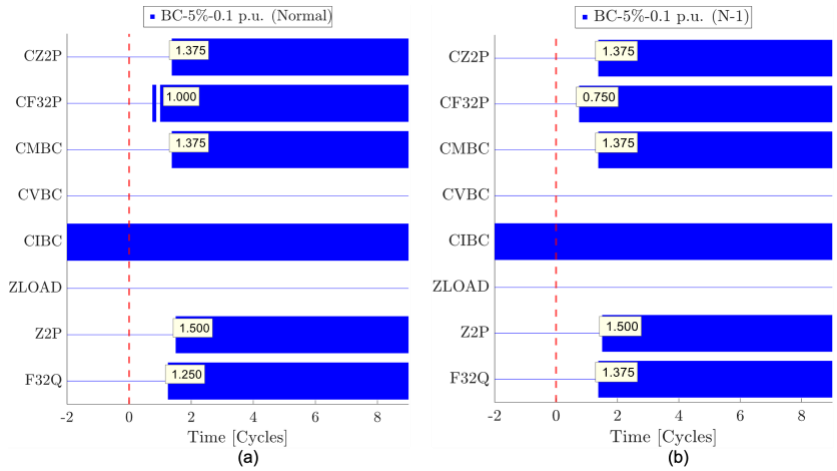


**Figure 39. R2 relay response with enhanced protection logic under normal and N-1 scenarios at L1**

Under grid conditions where synchronous generators dominate on both sides of the transmission line, whether in normal or N-1 scenarios, the enhanced logic demonstrated robust and rapid performance in conjunction with existing protection elements (Z2P, F32Q), as shown in Figure 39. In these scenarios, the fault current contribution from the synchronous generators led to a strong assertion of the phase overcurrent element (CIBC). Consequently, the custom zone phase element (CZ2P) was asserted within 1.375 cycles for normal scenarios (Figure 39 (a)) and 1.5 cycles for N-1 scenarios (Figure 39 (b)), followed by the correct identification of the forward fault direction by the positive-sequence directional element (CF32P). Meanwhile, the existing logic also asserted the distance element (Z2P) within 1.5 cycles for both cases, indicating that the enhanced protection scheme was as reliable as the existing settings. This confirms that the enhanced scheme maintains compatibility with traditional source-dominated grid characteristics, effectively using the available fault current for supervision while leveraging a stable positive-sequence angle for directionality.

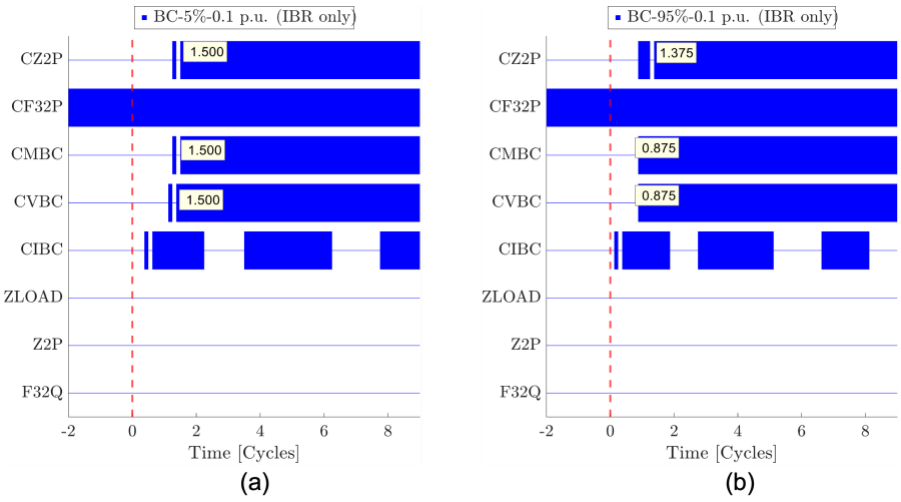


**Figure 40. R2 relay response with enhanced protection logic under the IBR-only scenarios at L1**

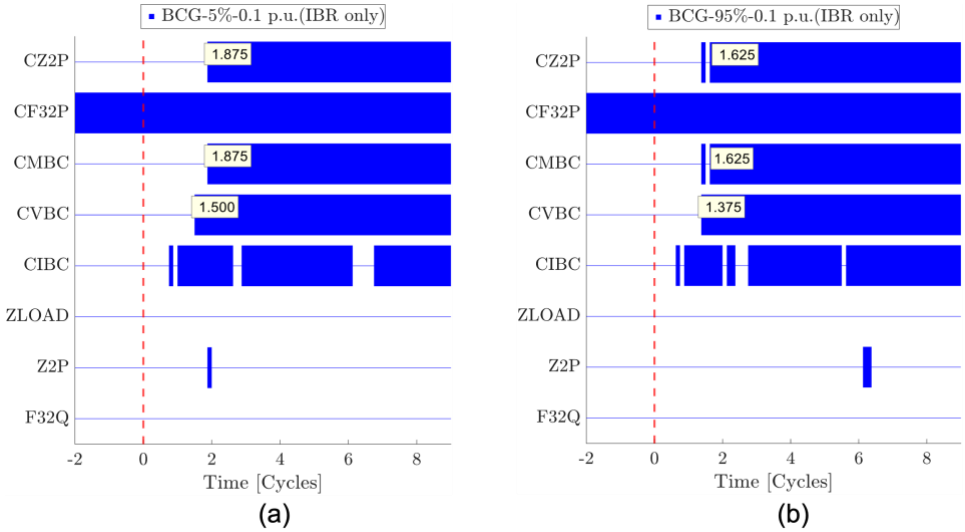


**Figure 41. R2 relay response with enhanced protection logic under the IBR-only scenarios at L2**

The critical validation of the scheme is demonstrated in the IBR-only scenarios, where the default negative-sequence logic failed to operate. Figure 40 (a) and (b) present the relay response for a phase-to-phase fault at 5% and 95% of L1 under the IBR-only conditions, respectively. In these scenarios, the adaptive undervoltage supervision element (CVBC) was successfully asserted by the distinct voltage sag characteristic of the weak grid environment. This voltage-based supervision is essential, functioning in parallel with the overcurrent element to ensure fault detection despite the lower or oscillatory current magnitude that is typical of IBR responses. Coordinated with the stable positive-sequence directional element (CF32P), the custom trip logic (CZ2P) operated reliably with an assertion time of 1.5 cycles for the zone 1 fault and 1.375 cycles for the zone 2 fault. A similar reliable performance was observed for faults on L2, as shown in Figure 41, where the logic successfully cleared phase-to-phase-to-ground (BCG) faults with an assertion time of 1.625 cycles for zone 1 faults (Figure 41 (a)) and 1.875 cycles for zone 2 faults (Figure 41 (b)). Collectively, these results confirm that the enhanced protection scheme

effectively bridges the gap between the traditional and IBR-dominated weak grid protection requirements, achieving 100% dependability across all tested fault types and locations.

## 4.4 Adding the Benchmark Inverter

A benchmark OEM inverter model was evaluated because both the GFL and GFM IBRs comply with IEEE Std 2800-2022 regarding the injection of negative-sequence current during unbalanced faults. The existing protection scheme was tested against this benchmark model under IBR-only scenarios. We tested two configurations of a benchmark inverter: one with a GFL only, equivalent in capacity to the primary OEM inverter, and another with one GFL and one GFM (GFL + GFM), both connected in parallel at the same point of common coupling in the system, each with a capacity equivalent to that of the primary OEM inverter.

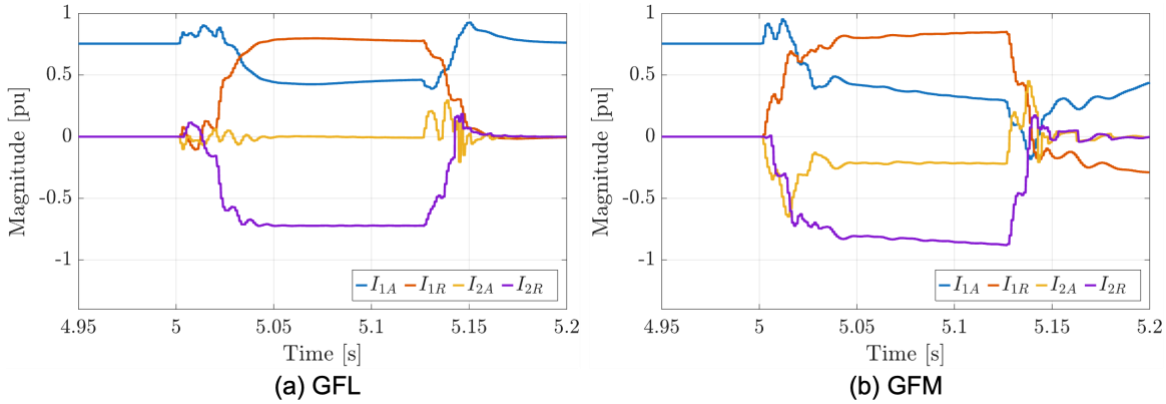


**Figure 42. Benchmark inverter fault current response under a BC fault**

The benchmark inverters demonstrated stable fault characteristics compared to the oscillatory response during the transient period of the primary OEM model. As shown in Figure 42 (a) and (b), both the GFL and GFM inverters maintained a stable negative-sequence reactive current component ($I_{2R}$) throughout the fault duration. More importantly, the negative-sequence reactive current ($I_{2R}$) is negative, and the negative-sequence active current ($I_{2A}$) is zero, which means that the negative-sequence current leads the negative-sequence voltage by 90° based on the formulas $I2A \coloneqq |I2|\cos(\angle V2 - \angle I2)$ and $I2R \coloneqq |I2|\sin(\angle V2 - \angle I2)$.

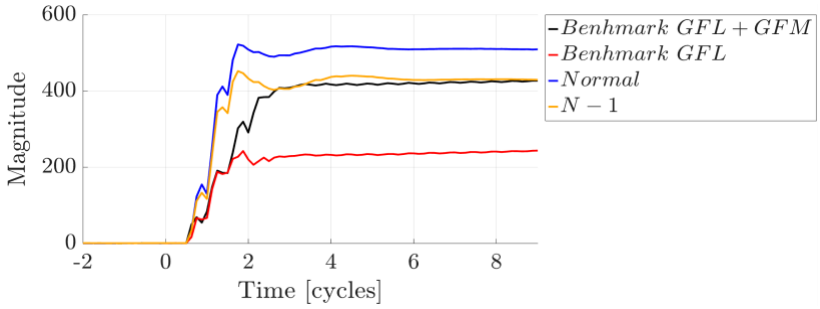


**Figure 43. Negative-sequence current ($I_2$) comparison during a BC fault**

Figure 43 confirms the provision of a regulated negative-sequence current ($I_2$). As shown in Figure 43, the benchmark GFL IBR contributes a good amount of stable negative-sequence current, and together the GFL and GFM IBRs inject a similar amount of negative-sequence current as the N-1 contingency condition. The reliable negative-sequence current injection is

further evidenced by the phasor relationship between negative-sequence quantities. Figure 44 (a) and (b) show that $I_2$ of both the GFL-only and GFL + GFM scenarios consistently lead $V_2$ by approximately 90° (appearing in the second quadrant relative to $V_2$) during the first, second, and third cycles of the fault. This consistent phase angle is critical because the calculation of Z2 relies on a stable phasor relationship to determine the directionality.

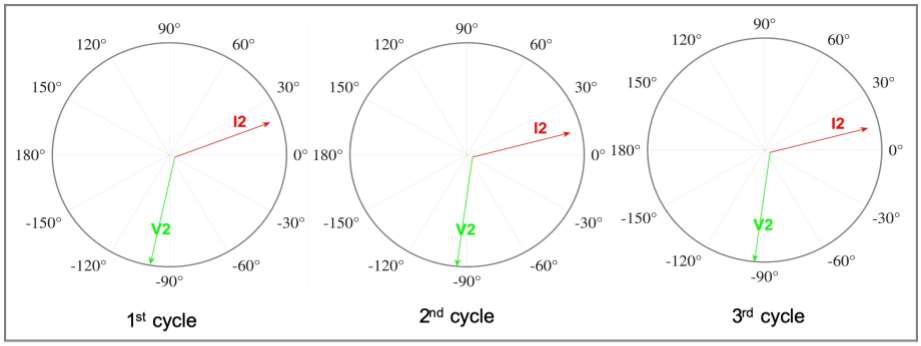


(a) GFL

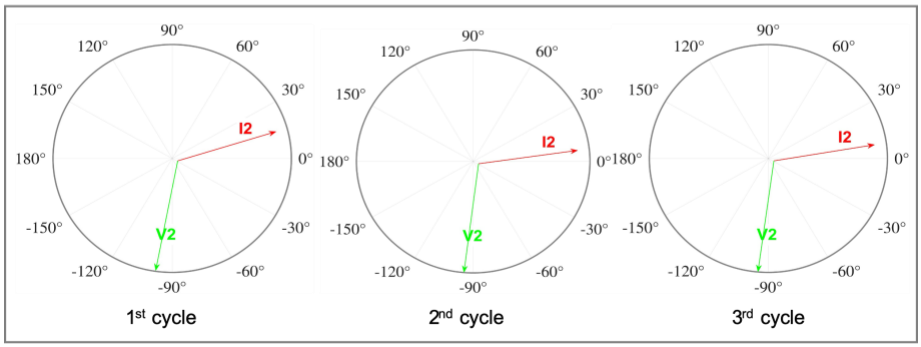


(b) GFL+GFM

**Figure 44. Phase angle of $\angle I_2$ and $\angle V_2$ under a BC fault**

Figure 45 shows the Z2 calculation for the 32Q element for both the GFL-only and GFL + GFM scenarios with the benchmark models. As shown in Figure 45 (a) and (b), the calculated Z2 remains stable and consistently stays below the forward threshold Z2FTH following the fault inception during faults with both the GFL and GFL + GFM under the IBR-only scenarios; therefore, the 32Q element can quickly indicate the forward fault, which also helps other elements supervised by 32Q to make decisions correctly and quickly.

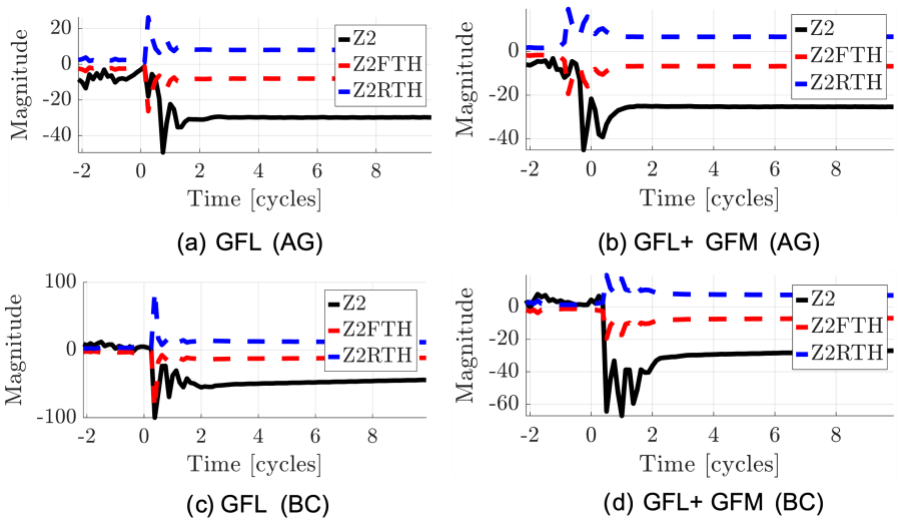


**Figure 45. Benchmark inverters' Z2 response during AG and BC faults**

In addition to directional stability, the benchmark inverters provide sufficient fault current magnitudes to activate the supervision elements. Figure 46 shows that the line-to-line fault current ($I_{LL}$) exceeds the overcurrent pickup threshold (Z50P.Set) within 0.5 cycles of the fault inception and remains above this threshold for the duration of the fault.

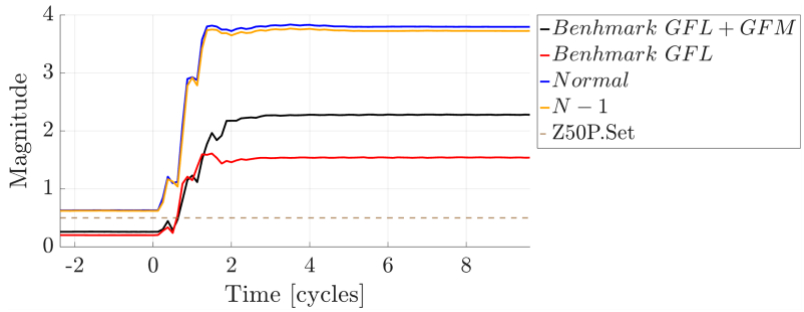


**Figure 46. Fault current comparison during a BC fault**

With a stable Z2 and sufficient $I_{LL}$, the default "QV" directional logic operated reliably. Figure 47 (a) and (b) show the R2 relay response for AG faults at 5%, 80%, and 95% of the fault locations for L1, with a 0.1-p.u. IBR power reference for both configurations (GFL and GFL + GFM). The directional element 32Q asserted within 1.00 cycle for all AG faults. Consequently, the zone 1 (Z1G) and zone 2 (Z2G) elements were asserted reliably within 1.0 cycles, except for AG faults at 5% of L1 under GFL-only scenarios, which required 1.125 cycles to assert the Z2G element.

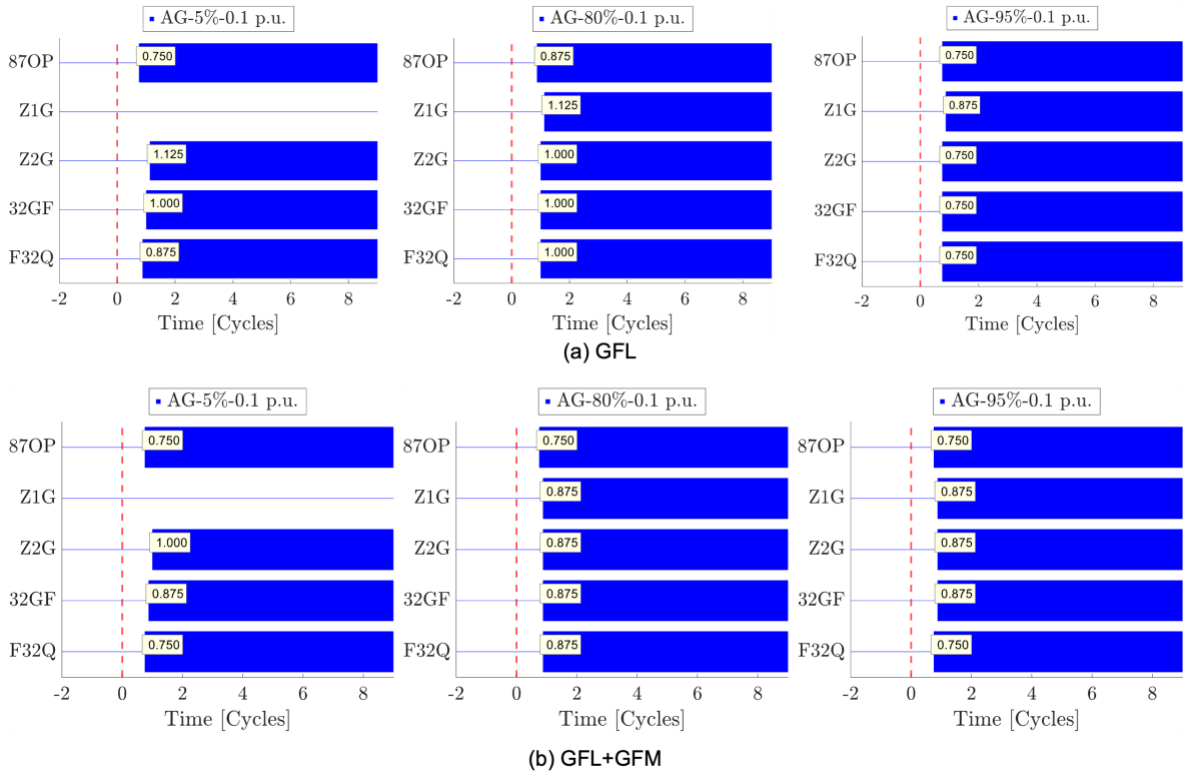


**Figure 47. R2 response with the benchmark inverter under the IBR-only scenarios during AG faults**

Similarly, with a stable Z2 and sufficient $I_{LL}$, the default "QV" directional logic reliably functions for phase-to-phase faults. Figure 48 (a) and (b) show the R2 relay response for BC faults at 5%, 80%, and 95% of the fault locations for L1, with a 0.1-p.u. IBR power reference for both configurations (GFL and GFL + GFM). The directional element 32Q asserted within a range of 0.625–1.125 cycles for all BC faults. Consequently, the zone 1 (Z1P) and zone 2 (Z2P) elements asserted reliably within 1.5 cycles. The GFL + GFM configuration demonstrated faster performance for zone 1 faults, asserting Z1P in 0.875–1.125 cycles, compared to 1.5 cycles for the GFL-only scenarios.

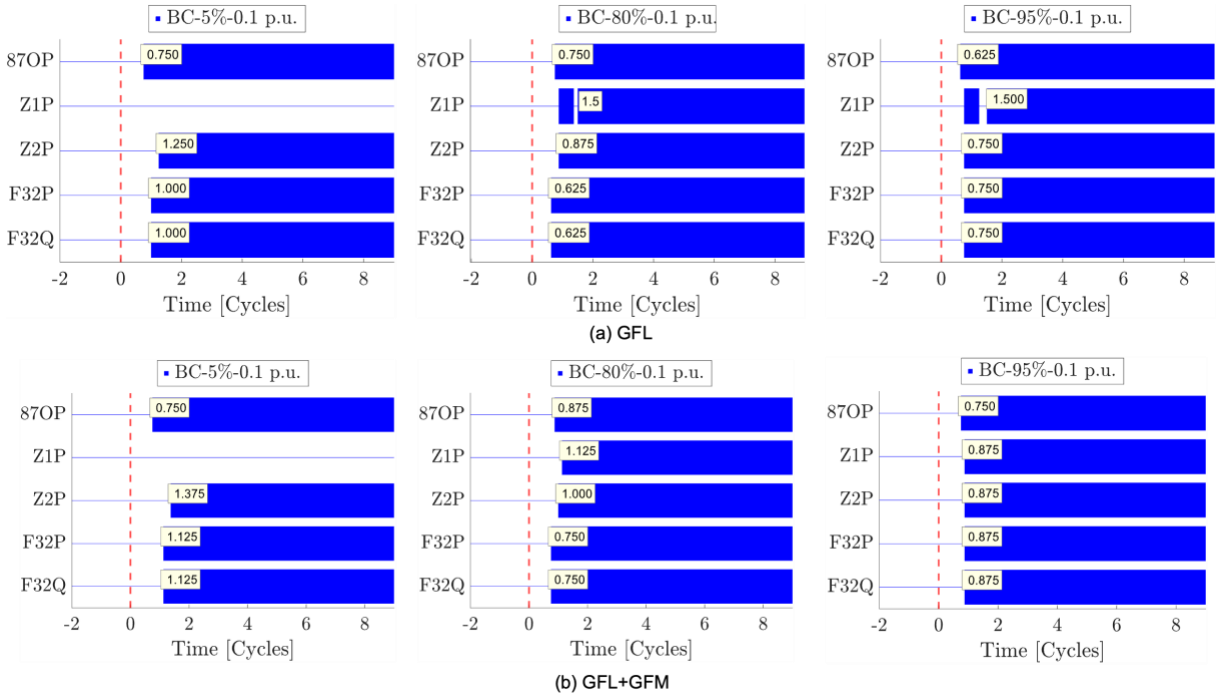


**Figure 48. R2 relay response with the benchmark inverter under IBR-only scenarios during a BC faults**

The comprehensive performance of the benchmark inverter for both AG and BC faults is summarized in Table 19. As detailed in Table 19, the existing protection elements operated reliably at all tested locations. In the GFL-only scenarios, the directional elements F32Q asserted within 0.75 to 1.0 cycles, allowing the zone 1 and zone 2 distance elements to clear faults within 0.75 to 1.5 cycles. The addition of the GFM inverter further enhanced the overall performance. In the GFL-only scenarios, during a zone 1 fault, Z1P was momentarily de-asserted (Figure 48 (a)), resulting in a final Z1P assertion taking 1.5 cycles. But with the addition of the GFM inverter, the decision was stable, and Z1P was asserted within 1.0 cycle without momentary de-assertion, providing a more reliable decision.

**Table 19. Summary of R2 Response With the Benchmark Inverter Under the IBR-Only Scenarios During AG and BC Faults**

| IBR Type | Element | AG 5% 0.1 p.u. | AG 80% 0.1 p.u. | AG 95% 0.1 p.u. | BC 5% 0.1 p.u. | BC 80% 0.1 p.u. | BC 95% 0.1 p.u. |
|---|---|---|---|---|---|---|---|
| GFL | **Z1G/Z2G/ Z1P/Z2P** assertion time (cycle) | Z2G: 1.125 | Z1G: 1.125 Z2G: 1.0 | Z1G: 0.875 Z2G: 0.75 | Z2P: 1.25 | Z1P: 1.5 Z2P: 0.875 | Z1P: 1.5 Z2P: 0.75 |
| | **F32Q/ 32GF** assertion time (cycle) | 1.0 | 0.75 | 0.75 | 1.0 | 0.625 | 0.75 |
| GFL+ GFM | **Z1G/Z2G/ Z1P/Z2P** assertion time (cycle) | Z2G: 1.0 | Z1G: 0.875 Z2G: 0.875 | Z1G: 0.875 Z2G: 0.875 | Z2P: 1.375 | Z1P: 1.125 Z2P: 1.0 | Z1P: 0.875 Z2P: 0.875 |
| | **F32Q/ 32GF** assertion time (cycle) | 0.875 | 0.875 | 0.875 | 1.125 | 0.750 | 0.875 |

The benchmark inverter provided a stable fault response with regulated negative sequence current compliant to IEEE Std. 2800-2022. Consequently, implementing a regulated negative-sequence current injection (compliant with IEEE Std. 2800-2022) in the primary OEM inverter constitutes a viable solution for restoring the reliability of the existing protection scheme under IBR-only conditions [7][8][9].

# 5 Conclusions and Future Work

This project conducted an EMT simulation-based fault study and laboratory protection relay CHIL evaluation of the existing protection scheme of our utility partner. The identified protection challenges are related to the IBR-only scenario and due to the GFL IBRs' lack of regulated negative-sequence current. Enhanced protection schemes (updated protection settings and customized protection logic) are proposed to tackle those challenges, and the validation shows the reliable operation of those enhanced protection schemes not only for the IBR-only scenario but also for the normal and N-1 contingencies. Additionally, another OEM provided IBR models (both the GFL and GFM inverters comply with the IEEE Std. 2800-2022 negative-sequence current requirement) that were used to replace the original OEM-provided GFL inverter, and the testing results show that there are no issues in the protection relay elements using this OEM-provided GFL inverter alone or with both the GFL and GFM inverters. The key learnings and findings are summarized as follows [12]:

- EMT simulation-based fault studies could become mainstream because of their capability in accurately representing the transients and dynamics of IBRs during faults. These needs will become more demanding when utility systems have high penetrations of IBRs and as they become the dominant source for fault current contribution. This work provides guidance on the process of obtaining a PSCAD model from the full CAPE model and how to resolve the key challenges, including: (1) There is no good practice to generate the equivalent area with IBRs for the reduced model. (2) There are floating transformer neutral issues. (3) The current of the non-faulted phase is not the same between the full and reduced model for unbalanced faults because of the presence of IBRs in the reduced network. (4) There is no transformer in the PSCAD library that can be used to set the zero-sequence impedance values directly.
- For transmission lines L1 and L2, the existing protection relays operate reliably under normal conditions and N-1 contingencies because the synchronous generators contribute a good amount of fault current and negative-sequence current under those scenarios.
- When the IBR is the only source contributing fault current, the differential element still operates reliably, but the distance and directional elements that rely on the regulated negative-sequence current and/or overcurrent mis-operate. The affected protection relay elements are: (1) 32 Q, (2) Z1P/Z2P/Z1G/Z2G, and (3) some overcurrent supervision elements. The inability of these elements to correctly assert stems from the lack of negative-sequence current and a consistent $I_2$-$V_2$ phasor relationship.
- The enhanced protection schemes address challenges of the lack of regulated negative-sequence current from IBRs. For ground faults, the increased restraining factors ($a_2$ and $k_2$) can quickly block the negative-sequence current-based direction element and switch to the zero-sequence voltage-based direction element; changing from the QV order to the V order has a similar effect but with a faster response because there is no waiting time for blocking the Q and switching to V. For phase-to-phase faults, the undervoltage and phase angle supervision elements are helpful to increase the selectivity and reliability of the mho distance element even with a low fault current. Those enhanced protection schemes are good references for other utility systems with similar problems.
- The second OEM GFL and GFM inverters both comply with the IEEE Std. 2800-2022 negative-sequence current requirement. In particular, the two models both provide a high amount of negative-sequence current, consistent negative-sequence current, and a

negative-sequence voltage phasor relationship. These are beneficial for relays to continue to operate reliably. That is why the directional and distance elements operate reliably with a fast response for both the GFL-only and GFL + GFM scenarios.

- In the real world, it is impractical for protection engineers to rerun fault studies and adjust the protection settings/logic to accommodate issues brought by IBRs. Requesting that the IBRs comply with IEEE Std. 2800-2022 is more doable. This should be included in interconnection studies and reviewed by protection engineers.

This project used only GFL IBRs for the fault study because GFM IBRs were not yet ready when the project was completed. We suggest that the original OEM vendors include negative-sequence current control in both their GFL and GFM inverter models and ensure that the fault responses under unbalanced faults comply with IEEE Std. 2800-2022 in terms of negative-sequence current magnitude, negative-sequence current leading negative-sequence voltage 90°~100° and setting time (≤4 cycles). Once these updated GFL and GFM IBR models are ready, we can rerun the fault study and CHIL evaluation. This will be the subject of future work.

# References


[1] J. Lewis Blackburn and Thomas J. Domin, Protective Relaying: Principles and Applications, Fourth Edition, CRC Press, 2014.

[2] S. Chakraborty, et al., "Studying the impact of IBR Modeling on the Commonly Applied in Transmission Line Protective Elements," *IEEE ECCE*, 2024.

[3] "IEEE standard for interconnection and interoperability of inverter-based resources (IBRs) interconnecting with associated transmission electric power systems," *IEEE Std 2800-2022*, pp. 1–180, 2022.

[4] Abu Shouaib Hasan, Yaswanth Velaga, Jing Wang, Lang Chen, Joseph Debeau, Andrew Arana, "Evaluating Protection System Performance for a Real-World Weak Grid Area with High Inverter-Based Resources," *IEEE PESGM*, 2026 (submitted).

[5] SEL-411L Advanced Line Differential Protection, Automation, and Control System Instruction Manual, Schweitzer Engineering Laboratories, 2023.

[6] Ryan McDaniel, Ritwik Chowdhury, Karl Zimmerman, and Brett Cockerham, "Applying SEL Relays in Systems with Inverter-Based Resources, SEL Application Guide," 2021.

[7] Jing Wang, et al., "Comprehensive Study of the Impact of Inverter-based Resources (IBRs) Modeling and Control in Protective Relay elements, *NREL Technical Report, TP-5D00-94430*, 2025, doi: https://docs.nrel.gov/docs/fy26osti/94430.pdf.

[8] P. H. Pinheiro, et al., "Analysis of Line Distance Elements for Various IBR Controllers and System Conditions," *Electrical Power System Research*, vol. 252, pp. 1-7, 2026.

[9] P. H. Pinheiro, et al., "Benefits and Recommendations for Using Classic Protection Functions in Transmission Lines Interfacing IBRs Compliant to IEEE 2800," in *CIGRE*, 2024.

[10] D. A. Tziouvaras, H. J. Altuve, and F. Calero, "Protecting mutually coupled transmission lines: Challenges and solutions," in *2014 67th Annual Conference for Protective Relay Engineers*, College Station, TX, USA, 2014.

[11] Craig Holt and Michael J. Thompson, "Practical considerations when protecting mutually coupled lines," in *2016 69th Annual Conference for Protective Relay Engineers (CPRE)*, College Station, TX, USA, 2016.

[12] Abu Shouaib Hasan, Jing Wang, Yaswanth Velaga, Lang Chen, Joseph Debeau, Andrew Arana, "Design Enhanced Protection Scheme for a Real-World Weak Grid Area With High Inverter-Based Resources," *IEEE Access* (submitted).

# Appendix A. Zero-Sequence Mutual Coupling

One recommendation from the protection studies (Section 4.2.1) is to change the "best choice ground directional element" setting from QV to V due to the lack of negative-sequence current in the severe contingency scenario where the inverter-based resource (IBR) is the only source for the relay. Controller-hardware-in-the-loop (CHIL) studies show that the zero-sequence voltage polarized element V can detect ground faults without any issues; however, zero-sequence quantities can be affected by mutual coupling. When more than one circuit shares the same right of way or shares a transmission tower, they are mutually coupled. These mutually coupled lines bring protection challenges [10][11]. The authors in [11] explained the modeling of mutual coupled lines and how they affect the zero-sequence direction-based protection elements.

Positive- and negative-sequence flux linkages with an adjacent line depend on the relative position of the phase conductors, but these linkages are low. So, positive and negative mutual impedances are practically zero for a perfectly transposed line. For un-transposed lines, these mutual impedances are low. Zero-sequence currents in one line due to the other line do not sum to zero, unlike positive- and negative-sequence currents. This mutual coupling can be visualized as a single-turn transformer in a zero-sequence network where the zero-sequence current in one line induces a current-dependent zero-sequence voltage on the adjacent line.

To understand the effect of a mutual coupled line, a parallel line to the entire length of L1 is assumed. Current lines in PSCAD are modeled as a PI line with positive- and zero-sequence impedances. To model mutual coupling, the tower geometry and conductor configuration are required. Based on the known line impedance, a fictitious tower geometry is developed (see Figure A-2.). Figure A-1.  shows the simplified one-line diagram of the L1 mutual coupled line.

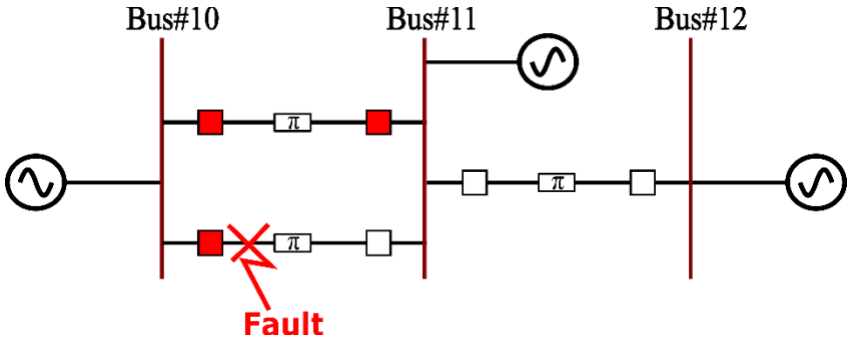


**Figure A-1. Simplified one-line diagram of the L1 mutual coupled line**

Under the severe contingency scenario, it is assumed that the parallel line is opened on the bus 11 end. A CHIL test is performed for phase-to-ground faults at three fault locations (5%, 50%, 95%) on the parallel coupled line. The relay did not see the fault due to the current being lower than the pickup threshold; therefore, the zero-sequence voltage polarized element V is secure with the mutual coupled line in operation.

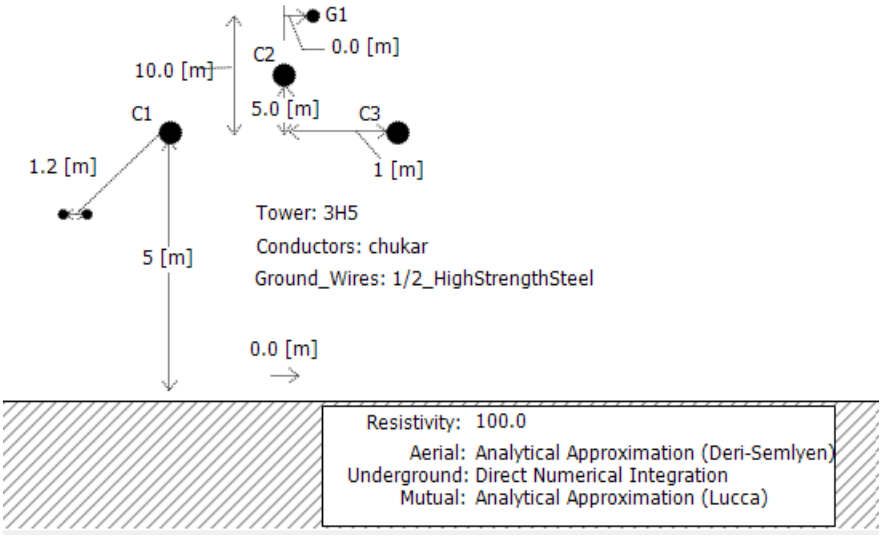


**Figure A-2. Fictious tower structure modeled in PSCAD**

# Appendix B. Inverter-Based Resource Fault Current

To further showcase the IBR fault current response, additional results are presented in Figure B-1.. Figure B-1. (a) shows the fault current response of the primary original equipment manufacturer (OEM) grid-following (GFL) inverter-based resource (IBR), and Figure B-1. (b) and (c) show the benchmark OEM GFL IBR and GFM IBR, respectively. The results show that the OEM GFL IBR did not generate regulated negative-sequence current in terms of magnitude and phase angle, but the benchmark OEM GFL and GFM IBRs both generated regulated negative-sequence current. In particular, the fault currents of the benchmark OEM GFL and GFM IBRs settle quickly for both the magnitude and phase angle, which are favorable conditions for the relays to make correct decisions.

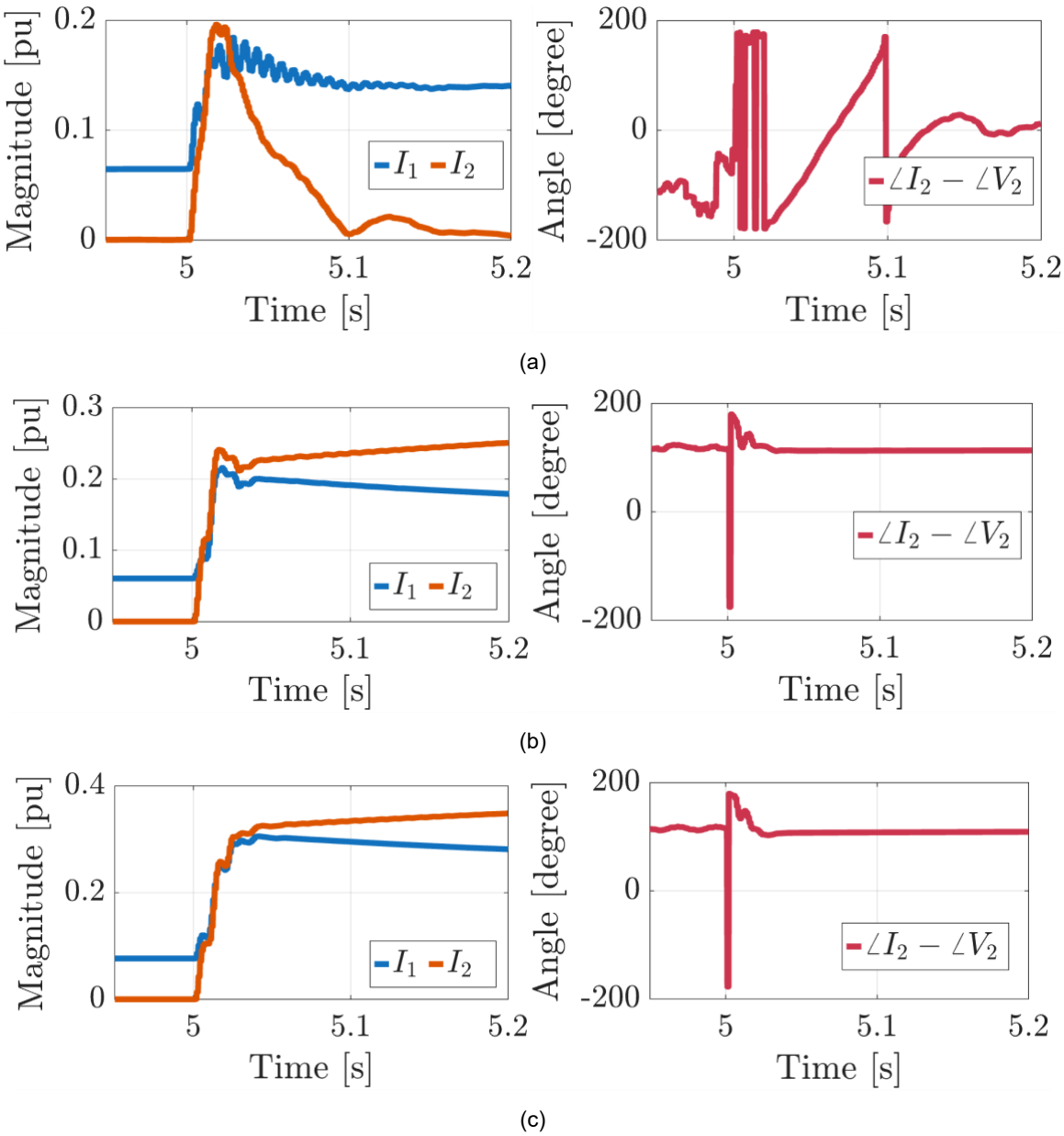


**Figure B-1. IBR fault current: I1 and I2 magnitude (left) and I2 and V2 phase angle difference (right): (a) OEM GFL IBR, (b) benchmark GFL IBR, and (c) benchmark GFM IBR**